INVESTIGATIONS OF MEDIUM WAVELENGTH MAGNETIC ANOMALIES IN THE EASTERN PACIFIC USING MAGSAT DATA

Christopher G.A. Harrison
University of Miami
Rosenstiel School of Marine & Atmospheric Science
4600 Rickenbacker Causeway
Miami, Florida 33149

September 30, 1980
Interim Report for Period June-September 1980

Prepared for
GODDARD SPACE FLIGHT CENTER
Greenbelt, Maryland 20771
(Magsat Investigations)

INVESTIGATIONS OF MEDIUM WAVELENGTH MAGNETIC ANOMALIES IN THE EASTERN PACIFIC USING MAGSAT DATA

1). Most of our effort during the first quarter has been to develop a set of computer programs for the analysis of the MAGSAT data. A list and description of these programs may be found in Appendix A to this report. The programs have been designed to be efficient in their use of CPU time.

2). A preliminary analysis of data collected in the eastern Pacific during the first two operational days of MAGSAT was done. A talk was given at the International Geological Congress in Paris, and the abstract for this talk (prepared before the data were available) is found in Appendix B. There is some long term discrepancy between the scalar field measured directly and that obtained from the vector sum of the three vector fields. This is illustrated in Figure 1, which shows the individual scalar fields and the field difference for one of the satellite passes over our area.

Another finding of some interest is the presence in some of the profiles of some fairly large amplitude anomalies. Some examples are shown in Figures 2 and 3. If these represent anomalies from crustal sources, this will be a finding of great interest. However, it is too early to say this at the moment. One possibility is that the anomalies are due to external sources. If this is the case, then further passes over the same area should not show the same anomalies. Or the anomalies may be part of the core field. In order to check on this possibility, the true wavelength of the anomalies must be determined. Since the core field probably becomes less than the crustal or mantle field at a spherical harmonic of degree about 13, anomalies of wavelength 1500 km or less (measured perpendicular to any lineation if the anomalies are lineated) probably represent crust or mantle sources. Again, the anomalies should be coherent from pass to pass over the same area.

3). A paper of relevance to the work which we propose to do using MAGSAT data has been submitted for publication in the Journal of Geophysical Research, and is included in this report as Appendix C.

4). We are now ready to commence a systematic analysis of data from the area of the eastern Pacific Ocean. The first step in this analysis will be to attempt to explain the observed magnetic anomalies at satellite altitude using a number of dipoles located within the crust of the Earth. An alternative which is to model the magnetization by uniformly magnetized tesseral caps located within the crust will also be tried and compared with the dipole results. The dipole data can be translated into magnetization data by specifying the total volume of material whose magnetization the dipole is supposed to represent.

The dipole or magnetization data can also be used to generated magnetic anomalies at a uniform height above the Earth. This will enable us to do Fourier analysis on these data, in order to compare the results with Fourier analyses done on data collected at the ocean surface (see Appendix C).

5). Total funds expended as of 30 September 1980 are $2390.25.

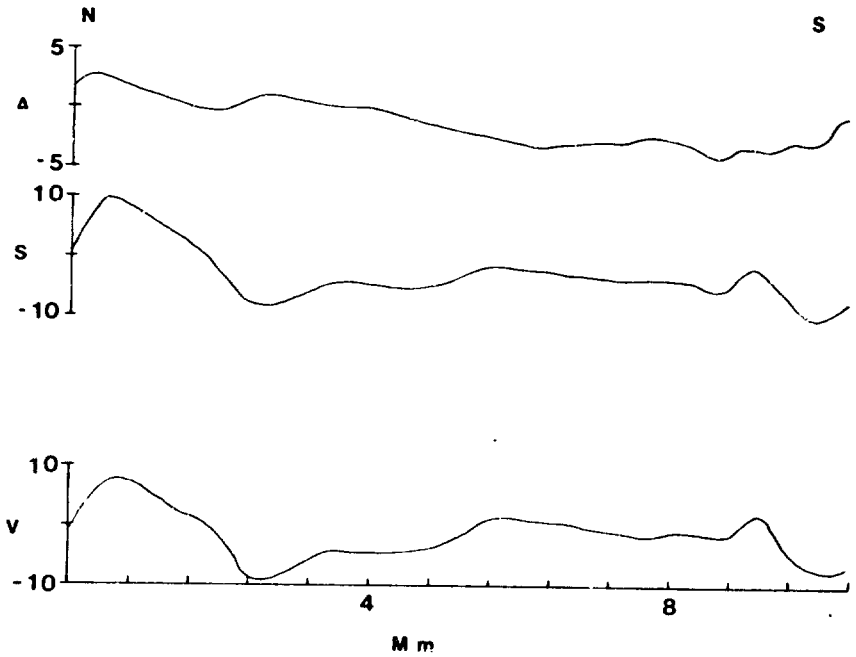

Figure 1. Comparison between three component vector and scalar magnetometers. The vertical scale is in nT. V is the total field calculated from the three component vector magnetometer. S is the total field recorded by the scalar magnetometer. The top curve is the difference between the two (S-V).

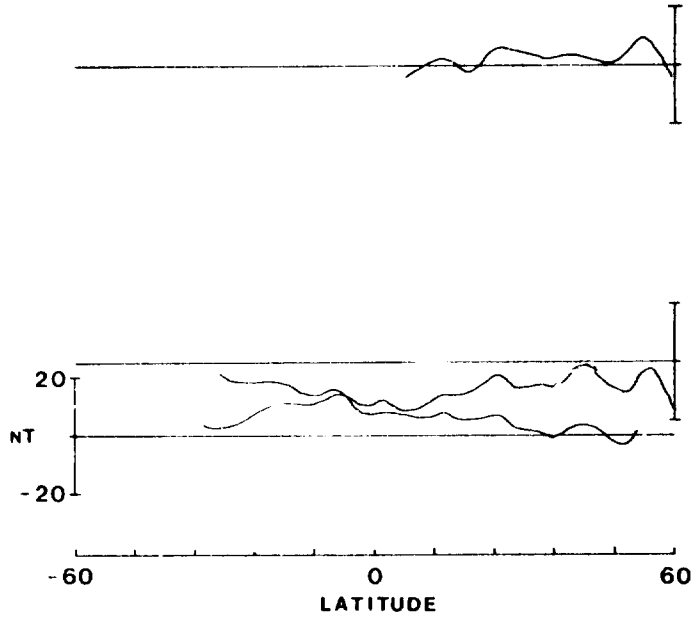

Figure 2. The total field recorded by the scalar magnetometer on three nearby passes. The vertical offset between the records is equivalent to the longitudinal difference between the passes. Correlations are much better between the closely spaced lines than between these two and the topmost line. The middle and top profiles are spaced about six degrees of longitude apart.

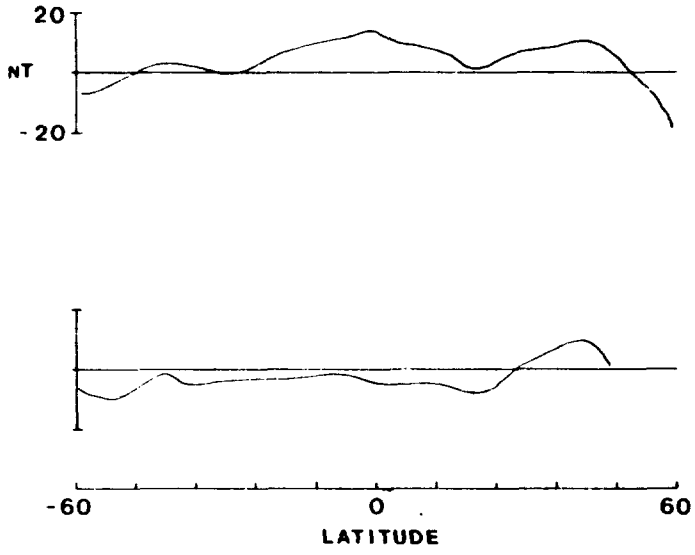

Figure 3. Total magnetic field recorded by two lines spaced about six degrees of longitude apart.

APPENDIX A

SOFTWARE PACKAGE

1. Program TAPERD
2. Program FILEUP
3. Program INVERT
4. Program MAGPLT
5. Program FLDPLT
6. Program FLDFIT
7. Program TRCPLT

PROGRAM DESCRIPTION

1. Program TAPERD (TAPE READ)

   translates NASA supplied EBCDIC tape and stores on disk.

2. Program FILEUP (FILL BREAK DOWN)

   sorts data into specified subfiles based on geographical boundaries supplied by user. Calculates and stores spherical coordinates and direction of main field for each data point resulting in substantial saving of computing in the inversion routine.

3. Program INVERT (FIELD INVERSION)

   calculates the matrix relating field measurement to equivalent source magnetization. Solves the matrix equation using the Crout varient of the Gauss-Jorden reduction. Provision is made for using either dipoles or spherical prisms as the equivalent sources merely by switching a subroutine, INVERT output magnetization matrix as a separate file.

4. Program MAGPLT (MAGNETIZATION PLOT)

   uses NCHAR contouring routine to plot the output of INVERT.

5. Program FLDPLT

   Uses the output of INVERT and expands the equivalent source array to a grid of field values at specified altitude. Contours, plots, and stores resultant field.

6. Program FLDFIT

   determines how well the calculated field matches the observed field. Produces a series of satellite track plots comparing calculated to to observed.

7. Program TRCPLT

   calculates, plots, and stores a magnetic profile at given altitude and orientation using the output from INVERT.

APPENDIX B

Abstract of Paper presented at International Geological Congress, Paris, July 1980.

Observations of long wavelength anomalies over ocean basins using MAGSAT data. Harrison, Christopher and Carle Mark, University of Miami, Miami, Florida, U.S.A.

MAGSAT data provide a useful means for studying the spatial arrangement of long-wavelength magnetic anomalies over the ocean basins. Previous work using satellites has demonstrated that such anomalies exist but has not come up with any definite solutions as to their source. We shall compare satellite data with ocean surface data by continuing upward the ocean surface data assuming, for the sake of convenience, that the ocean surface data are caused by lineated patterns of magnetization. We shall also study the spatial arrangement of long wave-length magnetic anomalies seen in the satellite data over the Eastern Pacific Ocean. In this region, the ocean surface pattern of magnetic anomalies is moderately well known, and so a direct comparison between the two types of data may be made. Hopefully the spatial pattern of the satellite anomalies may give us a clue as to their origin.. We shall also attempt to produce an equivalent source layer model for these magnetic anomalies. That is, we shall determine the magnetization variation within a layer of uniform thickness necessary to produce the observed anomalies. By comparing the values of magnetization within this layer with magnetizations measured directly on rocks thought to make up the oceanic crust and upper mantle, we should be able to delineate better the possible source region for the magnetic anomalies.

APPENDIX C
Submitted to
The Journal of Geophysical Research

Intermediate Wavelength Magnetic Anomalies over Ocean Basins

by C. G. A. Harrison and H. M. Carle, RSMAS, University of Miami, Division of Marine Geology and Geophysics, 4600 Rickenbacker Causeway, Miami, FL 33149

Abstract

We have examined three very long magnetic field profiles taken over ocean basins for the presence of long wavelength magnetic anomalies. The three profiles were one from the Atlantic Ocean in the TransAtlantic Geotraverse area, one running along latitude 35°S in the SE Pacific, and one running along 150°W in the Pacific. All three profiles show the presence of long wavelength magnetic anomalies generated in the crust or upper mantle. The analysis of magnetic field power spectra shows that the core field becomes unimportant at about a wavelength of 1500 km. Sea floor spreading anomalies should produce a maximum in power at about a wavelength of 65 km. Between these two wavelengths there should be a minimum in power which is not seen on observed records. Inverting the anomalous field to obtain some idea of the magnetization necessary to explain these long wavelength magnetic anomalies shows that values of magnetization in excess of 1 $A.m^{-1}$ are needed if the magnetized layer is as thick as the oceanic crust. Alternatively, rather large thicknesses of upper mantle material with lower intensities of magnetization need to be used. The reason why such magnetization variations exist is not known. It can be shown that upward continuation of the magnetic anomaly signature to an altitude of 350 km (about the perihelion altitude of MAGSAT) will produce anomalies up to 10 nT in amplitude. These should be capable of being seen by MAGSAT, and thus allow us to determine the spatial arrangement of the long wavelength anomalies, and hence, hopefully, a clue as to their origin.

Introduction

The presence of sea floor spreading magnetic anomalies in ocean basins has created great interest in the origin of these anomalies. Since they are one of the foundation stones for the revolution in Earth Science, a great deal of effort has been made in understanding their origin within the oceanic crust, and the types of geological, geophysical, geochemical and tectonic events which will tend to destroy or mask them. Consequently, little effort has been made in understanding marine anomalies not associated with sea floor spreading and reversals of the Earth's field. Anomalies of longer wavelength exist in the ocean basins, and require some source region within the oceanic crust or mantle. It is the purpose of this paper to describe these anomalies and to suggest constraints whcih may be used to determine their source.

Observations of Intermediate Wavelength Anomalies

Alidredge et al. (1963) published a magnetic profile of total magnetic field which was patched together from several different sources, but which went totally round the Earth. Although the path of the profile was not a great circle, its length was approximately the circumference of the Earth (40,000 km) because of the jaggedness of the path. On looking at the profile, it appears obvious to the naked eye that there are two components to the total magnetic field. One component is that generated in the core of the Earth which produces the very long wavelength signal of amplitude several tens of μT. The other is a signal which appears as a very short wavelength component on top of the long wavelength component, and has an amplitude of less than one μT and a wavelength of up to 100 km. Alldredge et al. explained these two types of anomalous field as being due to core sources (which produce the very long wavelength large amplitude signal) and crustal sources (which produce the short wavelength low amplitude wiggles). He concluded that the absence of intermediate

wavelength anomalies was due to the fact that the mantle, being in general above the Curie point of known ferromagnetic minerals, did not contribute to the magnetic anomaly pattern.

A subsequent Fourier spectral analysis done by Bullard (1967) of the same round the world magnetic field profile revealed a surprising thing. This was that instead of two regions of dominant power in the spectrum, the spectral energy started off high at the low wavenumber end of the spectrum, and fell rapidly with increasing wavenumber up to a harmonic of about 25 (representing a wavelength of about 1600 km) and then fell off much less rapidly with increasing wavenumber. As is fairly common, Bullard plotted the logarithm of power (ordinate) against wavenumber (abscissa). The absence of a minimum in power appropriate to mantle wavelengths was noted by Bullard, who also stated that a similar result was obtained along a line 60° long running from San Diego to Easter Island. Although some of the round the world profile goes across continental areas, much of it is oceanic, and subsequent results, to be described, show that the pattern is the same for purely oceanic paths.

Recently Nomura (1979) has also discovered that there are significant intermediate wavelength magnetic anomalies observed at sea level over oceanic basins in the western Pacific. He concluded that there must be significant sources for these magnetic fields within the upper mantle. Coles and Haines (1979) studied long-wavelength magnetic anomalies over Canada, and concluded that anomalies with sources within the lithosphere become dominant at spherical harmonic components above degree 13, a conclusion which we also reach from studying marine magnetic anomalies.

Long Profiles over Oceanic Basins

We have studied magnetic fields collected along long straight profiles in the Atlantic and Pacific Oceans. The locations of these profiles are shown in Figure 1.

The TAG profile is approximately 6000 km long and was collected during the TAG expedition (Lattimore et al., 1974). It runs almost exactly perpendicular to the magnetic lineations in the Atlantic having been designed that way. The SE Pacific profile was described by Keller and Peter (1968) and is approximately 11,000 km long. The maximum deviation of this profile from the perpendicular to the lineated sea floor spreading anomalies is about 28°. The north-south profile running at 150°W is approximately 13,000 km long and was kindly provided by Dr. B. Loncarevic of the Bedford Institute of Oceanography. Plots of the total magnetic field collected along these profiles are shown in Figure 2. In each profile, a total of 4,096 points has been digitized at equal spatial intervals. In each profile, it is possible to see the large smooth signal of field produced by core sources, and the small amplitude short wavelength component produced by crustal (or possibly mantle) sources. The Fourier spectra of all of these profiles show very similar features, which are now discussed.

We have performed fast Fourier analyses on all of the profiles shown in Figure 2. In order to do this we first removed a least squares linear trend from the data, and then subjected the resulting field to a standard fast Fourier transform. The squared amplitude (or power) for each harmonic is plotted in Figure 3 for each of the profiles. As is standard for such analyses, we have plotted the logarithm of power against wavenumber in radians km^{-1}. The presence of the large amplitude long wavelength core field can be seen in the large values of power exhibited by the first few harmonics for each profile. At higher wavenumbers, the power falls off slower with increasing wavenumber, showing that the depth to the sources producing the short wavelength component is less than those producing the long wavelength component (which we already know).

One of the problems of doing Fourier analysis on finite data sets is that the technique assumes that the data set is infinitely repeated, and so the final answer has to reproduce, for instance, the discontinuities between the beginning and end of the

record. One result is that if there is a large signal at one particular wavelength in the original record, the Fourier spectrum tends to smear out the signal over several of the surrounding spectral estimates. Now these records have large amounts of power at very long wavelengths, and it is probable that some of the power has leaked over into shorter wavelengths. One way out of this difficulty is to apply some sort of filtering to the data. Many such filters have been suggested. One of the most powerful is the 4π prolate spheroidal filter (Thomson, 1977). This filter is used in the space domain, and one result of applying the filter is that there is no discontinuity at the ends of the signal. The size of the filter is designed so that the total power in the signal remains the same. The trade off for any filter is that in order to make the leakage into frequencies far way from the central frequency very small, the width of the power peak associated with the central frequency becomes broader. However, the total power within each significant frequency peak remains about the same. All three signals have been subjected to the 4π prolate spheroidal filter and Fourier transformed. The resulting power spectra are shown in Figure 4. Comparison between these and the power spectra in Figure 3 shows that there is a much more definite division between the two portions of the spectrum. This is shown even more clearly in Figure 5, in which the power of the first few harmonics from all three profiles has been plotted. The separation between the steeply sloping power estimates (representing the core field) and the gradually sloping estimates (the mantle and crustal field) occurs at about a wavenumber of about 0.003 radians.km^{-1}. The slightly larger value for the TAG profile is probably because the profile is only about as half as long as the other two. There are fewer spectral estimates per unit wavenumber in this profile as in the other two. The broadening of the peak produced by the 4π prolate spheroidal filter takes place over an approximately equal number of spectral estimates, so that in the wavenumber domain, the peak appears to be broader for the shorter line.

Coles and Haines (1979) used a spherical harmonic representation up to degree 13 to separate core fields from the rest. Spherical harmonics of degree 13 have a wavelength of about 3,000 km, but this is for a potential, whereas the anomalies discussed above are obtained by measuring the intensity of the total field. In this case, the wavelength produced by degree 13 spherical harmonics is one-half that of the potential. This can easily be seen by discussing a dipole field, for which the potential is given by:

$$V = \frac{\mu_o}{4\pi} \frac{\underline{m}.\underline{r}}{r^3} \qquad (1)$$

where $\underline{m}$ is the dipole moment, and $\underline{r}$ is the position vector with the dipole as the origin. If $\underline{m}$ is an axial dipole and we calculate V along a line of longitude, then we get a wavelength of the circumference of the circle. However, the total field is given by:

$$T = \left[\left(\frac{\partial V}{\partial r}\right)^2 + \left(\frac{1}{r} \frac{\partial V}{\partial \theta}\right)^2 \right]^{1/2} \qquad (2)$$

where θ is the colatitude.

$$\text{Thus, } T = \frac{m}{r^3} \left[\sin^2 \theta + 4 \cos^2 \theta \right]^{1/2} \qquad (3)$$

This equation shows that there are two wavelengths of signal on going 360^o around a meridian of longitude. For higher harmonics, it is also easy to see that they produce wavelengths of total field equal to C/2n where n is the degree of harmonic and C is the circumference of the Earth. Consider the harmonic of degree and order n (a sectoral harmonic). The variation of potential around the equator is a function of sin $(n\phi)$, where ϕ is the longitude. The total field is equivalent to the square root of the sum of a constant term plus the square of the east-west horizontal field, which has the form of cos $(2n\phi)$. The resulting total field has 2n wavelengths around the equator. Thus, the wavelength of degree 13 spherical harmonics is about 1,500 km, which is very similar to the break in the curves shown in Figure 5.

At the high wavenumber end of the profile the power spectrum flattens out. This is noise. The slope of the power spectrum as a function of wavenumber can be used to determine the depth to the magnetic source (Spector and Grant, 1970; Harrison, 1976). The slope of the natural logarithm versus wavenumber is equal to -2z where z is the depth to the source region. Table 1 gives relevant information about the slope of the three spectra. It can be seen that the depths to the sources are about 4 km in the Atlantic and about 5 km in the Pacific. The interpretation of these results is complex, because we know that the depths to the oceanic crust, and so presumably to the source of the anomalies, varies considerably over each profile. In addition, the approximation is only valid for large wavenumbers. However, it can be seen from the power spectra (Figures 4 and 11) that the slope does not vary very much between wavenumbers where the core field becomes unimportant and wavenumbers where we start to get noise in the spectrum (about 1.2 radians.km^{-1} for the Atlantic profile and about 0.8 radians.km^{-1} for the EW Pacific profile).

Power Spectral Models for Marine Magnetic Anomalies

a) Crustal component. It is possible to determine the sort of power spectrum which might be expected from sea floor spreading anomalies. Suppose that the magnetization is confined to a horizontal layer whose upper surface is at a depth z, and whose thickness is h. Suppose also that the magnetization is uniform vertically through this layer and also in one horizontal direction (in other words, the magnetization is lineated). Suppose also that the magnetization is confined to be in one direction (or its reverse). This is a reasonable model for magnetization produced over a few millions of years, where the dipole field does not change with respect to the portion of oceanic crust, and where reversals are the major changes in the direction of the field. The magnetization can thus be expressed as a function which varies along an axis perpendicular to the lineation of magnetization. It can be Fourier analyzed to give

amplitudes and phases of harmonics. Schouten (1971) and Schouten and McCamy (1972) showed that a harmonic magnetization produced a harmonic field under these conditions, and also showed that the amplitude of the field was related to the amplitude of the magnetization by the following expression:

$$F(k) = M(k).C.2\pi\ (e^{-zk} - e^{-(z+h)k}) \qquad (4)$$

F(k) is the amplitude of the field at wavenumber k, M(k) is the amplitude of the magnetization, and C is a factor which depends on the directions of magnetization and regional field.

The factor C is given by:

$$C = [1-\cos^2 I.\cos^2(\alpha-D)]^{1/2}.[1-\cos^2 I_r.\cos^2(\alpha-D_r)]^{1/2}$$

where I and D are the inclination and declination of regional field, I_r and D_r are the inclination and declination of magnetization, and α is the declination of the lineation. We shall normally disregard any variation of C (which in fact lies between 0 and 1). Thus field amplitudes calculated from magnetization amplitudes will be overestimated, whereas magnetization amplitudes calculated from field amplitudes will be underestimated. The last term in the equation is known at the Earth filter (Schouten and McCamy, 1972). It has a maximum value as a function of wavenumber (or wavelength) which depends on z and h. Figure 6 shows the wavelength at which the Earth filter has a maximum value, and it can be seen that for any reasonable value of depth to the oceanic crust ($3.0 < z < 6.0$ km) and the thickness of the magnetized layer, assuming that the magnetization is in the ocean crust ($h < 6.0$ km) the maximum value of the Earth filter lies between wavelengths of about 20 and 50 km, which is equivalent to wavenumbers between about 0.1 and 0.3 radians.km^{-1}. Therefore, if the magnetization spectrum is white (equal at all wavenumbers) then the field spectrum should have a peak between 0.1 and 0.3 radians.km^{-1}.

As a comparison, the position of the maximum in power has been calculated using the method outlined by Spector and Grant (1970) in which an ensemble of individual sources is considered. Using a depth to the upper surfaces of the bodies of 4 ± 1.5 km, and an average thickness of 6 km, the maximum in power is found at a wavenumber of 0.14 radians/km, which is very close to that calculated using equation (4).

To derive the spectrum of the magnetization, we assume that the field reversals are caused by a Poisson process (Cox, 1968). It is then possible to calculate the power spectrum of the resulting magnetization (Rice, 1954; Harrison, 1976).

Examples of power spectra for various combinations of spreading rate and reversal rate are shown in Figure 7. In general it can be seen that the spectrum of magnetization is not white but that there is more power in the low wavenumber end of the spectrum. The spectrum is whiter if the spreading is slow and if the rate of reversals is high. Both of these conditions produce reversal boundaries which are separated by smaller distances, on average. A more general case of this phenomenon has been given by Spector and Grant (1970, Fig. 3).

It has been suggested that reversals do not obey a Poisson process but a renewal process (Naidu, 1971; Cox, 1975). In this sort of process, the probability of a reversal occurring varies with time since the last reversal. Immediately after a reversal, the probability is zero, and the probability rises with time to a finite value. The probability density function for one such process is given by:

$$P(\tau) = \frac{\lambda (\lambda \tau)^{K-1} \exp(-\lambda \tau)}{(K-1)!}$$

where λ is a reversal rate and K is a number equal to or greater than 1. The mean value is $\tau = K/\lambda$. If $K = 1$ the probability density function is exponential and the process is Poisson (Cox, 1975).

Naidu (1971) has calculated the power spectrum for such distributions of magnetization. This is given by:

$$S(w) = \int_0^\infty \frac{\sin^2(\frac{w}{2})}{\frac{w^2}{4}} P(\tau)d\tau$$

in terms of angular velocity w.

For K = 1

$$S(w) = \frac{2}{\lambda^2 + w^2}$$

and for K = 2,

$$S(w) = 2 \frac{w^2 + 3\lambda^2}{(w^2 + \lambda^2)^2}$$

Naidu (1971) found a value for K of 2 for the reversals occurring between 0 and 48 my. If we wish to compare the power spectra from distributions with different values of K, then it appears reasonable to make the average interval length equal (or the number of reversals within a certain time, the same). Thus if K = 1 and λ = 3 (per million years), we should compare this with K = 2 and λ = 6. This has been done in Figure 8, where it can be seen that the renewal process produces a spectrum which falls off less rapidly than does the Poisson process.

One reason why the reversal pattern may appear to be like a renewal process is because very short intervals of constant polarity may be missed in the record (Cox, 1968; Harrison, 1969). In this case the renewal spectrum should be compared with a Poisson spectrum with a slightly more frequent reversal pattern. The Poisson power spectrum for four reversals per million years is also shown in Figure 8, and it can be seen that there is very little difference between the two spectra. It would be difficult to determine from the spectrum of magnetization if the reversal process were Poisson or renewal, as a renewal spectrum would look very like a Poisson spectrum with a slightly greater reversal frequency.

The effect of the magnetization not having a white spectrum is to move the peak

of maximum power in the field signal to lower wavenumbers. However, this effect is not very great. It can be seen from Figure 7 that the maximum effect is to be found for a minimum reversal rate and a maximum spreading rate. Suppose we take a spreading rate of 100 km.my^{-1} and a reversal rate of 2.5 my^{-1} and calculate the wavenumber at maximum power of the field signal. Results indicate that this occurs at wavenumbers between 0.053 and 0.085 radians.km^{-1} depending on the crustal model used (see Table 1). For a more reasonable spreading rate of 40 km.my^{-1} and a reversal rate of 3.my^{-1} the maximum power is found between wavenumbers of 0.086 and 0.157 radians.km^{-1}.

Thus the crustal component in the field signal should give a maximum of power in the region of 0.1 radians.km^{-1} for any reasonable model of reversals and crustal magnetization.

b) Core field. Many different models of the core field have been produced. Two of the most recent, and therefore, the most accurate are those by Peddie and Fabiano (1976) and Barraclough et al. (1975) for the field at 1975.0. By using the method given by Lowes (1966) it is possible to calculate from the spherical harmonic coefficients of the magnetic potential the value of the mean square value of the field for each degree and order of harmonic. Summing these values up for each degree of harmonic and taking the square root gives the result shown in Figure 9. It can be seen that in the representation of the potential given by Barraclough et al. (1975) the contribution to the scalar field at the Earth's surface falls fairly uniformly with the degree of harmonic, if the RMS field is plotted on a logarithmic scale. It is commonly believed that if further harmonics of the core field could be calculated, they would continue to fall roughly on the straight line shown in Figure 9.

Any tendency for the values to fall significantly above such a line would mean that after extrapolation to the core mantle boundary, these degrees of harmonic would contribute more to the field than the lower harmonics (Lowes, 1974). In fact the line

shown in Figure 9 is less steep than a similar line calculated by Lowes (1974), which means that power of the field at the core-mantle boundary is more evenly distributed over the first few degrees of harmonic than suggested by Lowes (1974). Cain (1975) produced a plot of power versus degree of harmonic for POGO data. In his plot, the harmonics between 9 and 12 lay above the straight line through harmonics between 2 and 8, and he suggested that possibly at degree 9 there appear non-core sources, and that certainly at degree 13, non-core sources start to dominate the surface field.

c) Combination of core and crustal sources. The core sources seen in any one profile are not necessarily going to be similar to the summation of core sources which went into constructing Figure 9. However, it is instructive to see what an average core source would do to a single total field profile. Lowes (1974) has shown how it is possible to transform spherical harmonic information into total field information gathered along a profile. The method is only strictly valid for harmonics much higher than the dipole field harmonic. But the result of doing the transformation for spherical harmonics of degree four and higher from Barraclough et al.'s (1975) model is shown in Figure 10. The points on this line should in fact be shifted downward compared to the points from the three profiles. This is because the three profiles have fewer estimates of power per unit wavenumber than does the spherical harmonic analysis. We should not expect too good an agreement between the spherical harmonic analysis and the individual profiles, because the power of these latter can only be approximately estimated using the 4 πprolate spheroidal filter. However, there is no doubt that the core field becomes insignificant at about a wavenumber of 0.003 radians.km^{-1} for the two longer profiles, and at about 0.004 radians.km^{-1} for the shorter TAG profile.

As we have seen, the crustal sources should give a peak in the spectrum in the region of 0.1 radians.km^{-1}. In order to model the spectrum from crustal sources, we have made the power equal to e^4 at a wavenumber of 0.1 radians.km^{-1}, which is

approximately what it is for the EW Pacific spectrum shown in Figure 4. Two models for the crust are shown, and it can be seen from Figure 10 that there is a definite reduction in power at low wavenumbers before the core field power begins to take effect at about 0.005 radians.km^{-1}. This low in the power spectrum is not present on any of the three spectra shown in Figure 4. The implications of this are discussed in the next section.

An alternative way of presenting a comparison is to plot the theoretical spectrum on top of one of the observed spectra from Figure 4. This comparison is shown in Figure 11. The full smooth line is for a model in which the reversal rate is 3.my^{-1}, the spreading rate is 30 km.my^{-1}, the depth of the top is 5 km and the depth to the bottom is 11 km. The dashed line is for a reversal rate of 4.my^{-1}, a spreading rate of 25 km.my^{-1}, a depth to the top of 5 km and a depth to the bottom of 5.5 km. The first represents a model in which the whole of the oceanic crust is involved, whereas the second represents a model in which only the top 500 m of oceanic crust is producing magnetic anomalies. All three profiles were made to agree at a wavenumber of 0.15 radians.km^{-1}. It can be immediately seen that the calculated spectrum from the thin layers does not fit the observed spectrum as well as that from the thick layer. If agreement between the spectrum from the thin layer and the observed spectrum is made at a higher wavenumber, the fit at the low wavenumber end becomes even poorer.

Inversion of Field to Obtain Magnetization

We wish to obtain some idea of the magnetization which might be responsible for the field in the three profiles. In order to do this, we just use the inverse of the process outlined by equation 4. In other words, we divide the amplitude of each field spectral estimate by the Earth filter, remembering that since we assume that C is unity, the magnetization amplitude will be a minimum estimate. The inverse of the

Earth filter has a minimum at around 0.1 to 0.3 radians.km^{-1} for all reasonable models of crustal magnetization, and so amplitudes of estimates with low or high wavenumbers become amplified more than do the amplitudes of the estimates of intermediate wavenumbers.

When trying to obtain magnetization from magnetic field, it is obviously impossible to use a 4π prolate spheroidal filter on the data before taking a Fourier transform, because then the resulting magnetization will also have the filter included in it. Comparison of Figures 3 and 4 suggests that it is impossible to obtain a good picture of the low wavenumber portion of the crustal field in the presence of the large core field by doing a simple Fourier analysis. We are therefore constrained to removing the core field before analysis. The regional fields removed were derived from the IGRF. Figure 12 shows the anomalous field for each profile after having removed the regional (core) field. Figure 13 shows the Fourier spectrum of the three anomalous field signals. Comparison between this figure and Figures 4 and 5 shows that the overall level of power is similar, except for the large core field signal which is seen in Figures 4 and 5, but not in Figure 13. We are thus confident that removal of the regional field has not resulted in any undesirable increase in power at intermediate wavelengths. In any case, the filtering which we apply to the data before inversion, to be described below, will certainly take care of any residual core field left after removing the regional fields.

Another problem which has to be taken care of is that the spectral estimates continue out to wavenumbers of about 1 radian.km^{-1} for the longer profiles and about 2 radians.km^{-1} for the TAG profile (equivalent to wavelengths of about 3 and 6 km). When these amplitudes are multiplied by the inverse Earth filter, they give very high amplitudes in the magnetization. The inverse Earth filter is about 6000 times as great at a wavenumber of 2 radians.km^{-1} as it is at a wavenumber of 0.1 radians.km^{-1} for a crustal model in which the magnetization is limited to a layer between 5 and 11 km

from the observation level. This problem was first recognized by Bott (1967). Bott and Hutton (1970) used a matrix method to invert magnetic field observations to obtain magnetizations of blocks of crust of uniform width. They showed that if the width of the block is less than about half of the depth to the surface, then the magnetization contrasts between individual blocks becomes very large, and no coherent pattern is produced. Thus resolution is limited to a wavelength of about the depth of the ocean or about 5 km, corresponding to a wavenumber of about 1.25. By studying the power spectrum of the field, it is possible to see that at high wavenumbers the spectrum flattens out, especially for the TAG and EW Pacific data shown in Figure 4. It is thought that this is where noise begins to predominate. For the EW Pacific profile, the noise begins at a wavenumber of about 1.0 radians.km^{-1}. In order to make sure that little of the observed signal associated with noise is used to generate spurious magnetization, no wavenumber above 1.0 was used in the inversion. A cosine taper was applied to wavenumbers between 0.5 and 1.0 radians.km^{-1}, along the lines suggested by Schouten and McCamy (1972). For the lower wavenumber end, a similar scheme was adopted. In order to make sure that no core field was involved in the magnetization, harmonics with wavenumbers less than 0.004 radians.km^{-1} were not used at all. A cosine taper was applied to wavenumbers from this value to twice this value. This band pass filter is very conservative, in the sense that we are definitely cutting off considerable power generated in the crust or upper mantle at either end.

Magnetizations calculated in this way are shown in Figure 14. We have chosen to use a crustal model in which the whole of the crust is magnetized. In other words, the depth of the top of the magnetized bodies was assumed to be 5 km and their thickness was assumed to be 6 km. We must first emphasize that this figure is somewhat schematic. For instance, we have not phase shifted the harmonic components. This means that we are assuming that the phase filter of Schouten and McCamy (1972) is equal to zero. That is, we assume that the magnetization is vertically downward and

that the regional field is also vertically downward. Also, the magnetizations are minimum values for the reasons discussed above.

It can be seen from Figure 14 and Table 2 that the Atlantic magnetizations are considerably less than the magnetizations obtained from the Pacific profiles. This is at first sight odd, as the power spectrum for the Atlantic anomalous field (Figure 11) looks about the same as the other two. However, since the profile is only about half the length, there are only about half the number of spectral estimates per wavenumber increment in the Atlantic profiles as in the other two, and so when a magnetization is reconstructed from the anomalous field, this becomes about half the size. This is discussed in greater detail below.

The interesting point about this figure is the very large magnetizations necessary to produce the observed magnetic anomaly if the source is confined to the oceanic crust. Peak values of several $A.m^{-1}$ are necessary. Table 2 shows average values of magnetization for each line. Another interesting thing about the figure is that the magnetizations necessary to cause the sea floor spreading anomalies (the short wavelength wiggles which can be seen in Figure 14) are often smaller than the magnetizations necessary to cause the long wavelength anomalies. Thus, for the model described, the sea floor spreading anomalies are sometimes produced by magnetization contrasts which do not produce reversals of magnetization. Of course other models could be proposed for which this statement is not true. For instance, the sea floor spreading anomalies could be modelled by a thin layer at the surface of the oceanic crust, and the long wavelength anomalies could be caused by deeper sources within the crust and mantle.

If the thickness of the magnetized layer is smaller than the 6 km figure used to generate the profiles shown in Figure 14, then the magnetization will increase correspondingly. It can be shown that for long wavelength features, the magnetization is inversely proportional to the thickness. It is also independent of the depth, provided

that the depth is not too great. These approximations are good provided that zk is less than about 0.1 and and hk is less than about 0.4 (see equation4). Thus they are true for much of the longer wavelength signal seen in Figure 12. Suppose for instance that the short wavelength sea floor spreading signal came entirely from the crust, and that the longer wavelength signal came from a layer of serpentinized mantle which originally lay below the Moho (Lewis and Syndsman, 1977). Thus if this layer were 1 km thick, the magnetization variation would have to be about six times that show in Figure 12. An alternative way of producing anomalies would be to have a layer of varying thicknesss but constant magnetic susceptibility, carrying an induced magnetization produced by the core field. This is an attractive hypothesis in some ways, because it does not require the serpentinite to carry any coherent remanent magnetization. Some serpentinites can have high values of susceptibility. For instance, the average susceptibility of the serpentinites studied by Fox and Opdyke (1973) was 0.0415 (S.I.). With such a susceptibility, and with a field strength of 50 μT, the magnetization becomes 1.65 $A.m^{-1}$. This is very roughly equivalent to the largest magnetizations shown in Figure 12, and thus variations in thickness of about 6 km would have to exist for the magnetic anomalies to be explained by rocks of constant susceptibility. Alternatively, the rocks could vary in susceptibility, as not all serpentinites have such a large susceptibility (see for instance the results given by Irving et al., 1970), but the total thickness of the serpentinite layer of varying susceptibility would have to be about 6 km.

The data presented by Lewis and Syndsman (1967) suggest that there is a low velocity zone at the base of the oceanic crust. Part of the evidence for this is a finite time delay between the critically refracted ray travelling through layer 3, and the reflected ray from the Moho. For line 8, this delay is about 0.31 sec, and this allows us to calculate the thickness of the low velocity zone if we assume that it has a certain velocity. Simple calculations show that for an assumed velocity of 6.5 $km.sec^{-1}$ the

layer would have to be 1.84 km thick, and that for an assumed velocity of 6 km.sec^{-1} the thickness would drop to 1.3 km. Judging from the work of Saad (1969) and Hatherton (1967), the density at which partially serpentinized peridotite becomes highly susceptible is 2.7 to 2.8 Mg.m^{-3}, at which density the P-wave velocity is between 5.5 and 6 km.sec^{-1} (Christensen, 1972). It therefore appears unlikely that the time delays measured by Lewis and Syndsman (1967) permit a thick enough layer of serpentinite at a low enough density to contribute significantly to the long wavelength portion of the magnetic anomalies measured over oceanic basins.

The Effect of Diurnal Variation

Diurnal variation of the Earth's field can be several tens of nT in amplitude, and occurs over a wavelength equivalent to the distance a ship goes in a day, or about 450 km. This is equivalent to a wavenumber of 0.014 radians.km^{-1}, and is thus a potential source of error in the work described above. If there is a significant component of external field signal in the low wavenumber portion of the record, then our values of magnetization may be too high, if we regard this external portion as being caused by a variation of magnetization. We have checked the magnitude of this effect for the EW Pacific profile and found it to be negligible. We took the magnetic field record from Toolangi in eastern Australia for the duration of the EW survey, taking into account the difference in longitude between the beginning and end points of the survey, and the station at Toolangi, which is at about the same latitude as the survey. We then digitized this record over 4096 equally spaced time intervals and did a fast Fourier transform on the resulting signal. We then assumed that the signal represents an external magnetic field collected at uniform intervals of distance along the EW Pacific survey. This is not strictly true, because the ship did not go at a uniform speed, but for purposes of seeing whether significant external power is present, it is an acceptable method. Then the power of the Fourier transform can be

represented as a function of wavenumber. The original total field record from Toolangi, and its power spectrum are shown in Figure 15. It can be seen that significant peaks are produced, these representing signals with a period of one day plus the second and third harmonics of this signal. These three peaks produce power which just overlaps the lower levels of power shown for the EW Pacific profile at the appropriate wavenumbers, but the average power level of the Toolangi record is several factors of e less than that seen in the profile, meaning that there is little contribution from the external field to the observed signal, a conclusion also reached by Nomura (1979).

Extrapolation to Satellite Altitudes

The artificial satellite MAGSAT is due to be launched in late 1979, and it should provide a good opportunity to study the spatial arrangement of the long wavelength magnetic anomalies. In order to determine the signal likely to be generated at the satellite altitude, we have taken the observed field anomaly signals from the three profiles and continued them upward to 350 km altitude, the approximate perihelion distance of MAGSAT. In doing this, we have had to assume that the anomalies are lineated perpendicular to the line of the profile, which is not necessarily true. One useful consequence of upward continuation is that it acts as a nice low pass filter, and allows us to see very easily the shape of the long wavelength signal. These upwardly continued fields are shown in Figure 14, along with the bathymetry along each profile, with various topographic features marked along these depth profiles. In doing these upward continuations we have rejected the first few harmonics and have applied a cosine taper to the next few, in much the same way as was done to generate magnetization values. This is a conservative approach, in that we have probably rejected some of the crustal magnetization signal at the low wavenumber end of the spectrum. Addition of more of the lower harmonics would increase the signal seen at

satellite altitudes considerably, as these lower harmonics are not as attenuated as the higher ones.

Discussion

In order to understand more fully what is going on in these long wavelength magnetic profiles, we compare the results from each of the profiles. To do this most effectively, we have calculated total power over each 0.05 radians/km^{-1} interval (or over each 0.02 radians.km^{-1} interval below 0.1 radian.km^{-1}). We have done this for three different power spectra. Firstly, the power spectra shown in Figure 4 are plotted in Figure 17a. This is the power generated from the total field signals, but we have not plotted the power between 0 and 0.02 radians.km^{-1}, as this would be very high with respect to the rest of the power since it contains almost all of the core signal. The power generated from the regional field (total field minus IGRF) after multiplying by the 4π prolate spheroidal window is shown in Figure 17b, and the power from the regional field with a box-car data window is shown in Figure 17c. The least squares regression lines of power against wavenumber are also shown. They have been calculated from 0.05 radians.km^{-1} to where the lines stop. The slopes and intercepts of each of the these lines are given in Table 3. There are significant changes in the power spectra for each type of treatment. The intercept for the EW Pacific profile decreases by 0.5, whereas that for the NS profile increases by the same amount and that for the Atlantic profile stays very constant. There is a general tendency for the negative slope to decrease as well, giving more relative power at higher wavenumbers.

The magnetization values were derived from the spectra shown in Figure 17c. Since the NS and EW Pacific profiles have very similar power spectra it is not surprising that they have similar RMS values of magnetization. The Atlantic profile has a spectrum which is about a factor of e less than the two Pacific profiles, and so one would expect that its RMS magnetization would be about $\sqrt{e}$ less than the two

profiles, whereas it is in fact about a factor of 2.2 less.

The average magnetization value for the Atlantic profile would be very similar no matter what signal was used to generate it, as the power in the signals is similar. The average magnetization of the EW Pacific profile would be greater if either of the other two spectra had been used to generate it, since these spectra are larger than the one actually used up to wavenumbers of 0.67 radians.km^{-1} for the regional field with the 4π prolate spheroidal data window, and 0.5 radians.km^{-1} for the total field. However, the magnetization for the NS profile would be smaller if either of the other two data sets had been used, since they both have smaller intercepts and steeper negative slopes. Based on this argument, we suggest that the magnetization of the EW profile shown in Table 2 is a minimum value, and that the magnetization for the NS profile is a maximum value, whereas that for the Atlantic profile is approximately correct.

It is possible to estimate what would be expected from each profile, at least as regards the portion of the signal generated by sea floor spreading magnetization contrasts. The EW profile crosses sea floor spreading anomalies over about two-thirds of its length. At the western end of the profile it is crossing the Cretaceous quiet zone, in which the anomalies should be suppressed. The lineations to the east are approximately perpendicular to the profile (RMS angle from the perpendicular is 11°). The NS profile on the other hand is never running perpendicular to the lineations. For the southern 14% of the profile, it is running at about 40° to the lineations and crosses the Pacific-Antarctic ridge at the extreme southern end of the profile. For the middle 57% the profile crosses oceanic crust formed during the Cretaceous quiet time. The northern 29% of the profile crosses areas of lineated magnetic anomalies, but the anomalies trend within 10° of the direction of the profile. Thus we should expect that the EW profile should have much stronger average magnetization, since it is crossing many more lineations, and the lineations are more perpendicular to the profile. This

confirms our hypothesis that the magnetization shown in Table 2 are minimum ones for the EW profile and maximum ones for the NS profile.

The Atlantic profile is everywhere perpendicular to the lineations where they exist. This is due to the design of the TAG experiment. The Teritary and Mesozoic lineations occur over about half the length of the Atlantic profile, which is a slightly smaller percentage than for the EW Pacific profile, but not enough to cause the factor of $\sqrt{e}$ difference in power. A reason must be sought in the relationship of the lineations to the dipole field during the time that the various portions of the oceanic crust were being created, and on the geometry of the lineations with respect to the field. Magnetizations running parallel to the lineations have no effect on the external field, except at fracture zones. So we must calculate the component of field within a plane perpendicular to the horizontal direction of lineation. If we make the assumptions that the average paleolatitude of the TAG profile is 25°N, and that the average declination of lineation with respect to the paleolongitude at the time of formation of the lineation is 30°, then the component of field in this plane is 0.959, for an equatorial field of unity. If the average paleolatitude of the EW Pacific profile is 40°S, and the average declination is 10°, then the component of field in the plane is 1.292 or a factor of 1.347 higher than for the Atlantic profile. Since lineations cover two thirds of the EW Pacific profile and only one half of the Atlantic profile, there is another factor is 1.333 to take into account, resulting in an overall factor of 1.8, which is quite close to the $\sqrt{e}$ deduced from Figure 17c.

Another result of some interest is also illustrated in Figure 17a. This is that the wavenumber at which each of the profiles begins to show noise is different. The lines on the figure represent the best fitting line to the power estimates starting at 0.05 radians.km^{-1} and going up to the highest wavenumber for which the power continues to fall on a straight line. This occurs at a wavenumber of 0.8 radians.km^{-1} for the EW Pacific profile. For the NS Pacific profile, this level is not reached, as there is no

tendency for the slope of power as a function of wavenumber to flatten out. Not all the points for the Atlantic profile are plotted in Figure 17a. Since the field measurements are more closely spaced in the Atlantic profile than in the two Pacific profiles the power estimates continue to higher wavenumbers. But the values of power above 1.2 radians.km^{-1} average about 0.5, and so it is clear that 1.2 radians.km^{-1} marks the point at which noise starts to predominate. We are unable to explain why this is a factor 50% greater than a similar point for the EW Pacific profile. Noise starts to predominate at a slightly higher wavenumber for the other two spectra of the EW Pacific profile (Figures 17b and 17c).

Conclusions

From an analysis of three long total magnetic field profiles taken over ocean basins, and from a consideration of previously published material, it is found that there is a significant signal in the wavelength range of 1500 to 150 km. This is too short a wavelength to be caused by the core field, which becomes insignificant at about a wavelength of 1500 km; this intermediate wavelength signal is not caused by a typical sea floor spreading process, which should give maximum power in the wavelength region about 50 km. It has been shown that the external magnetic field contributes very little to this intermediate wavelength signal. Efforts to explain the cause of this signal have so far failed. It appears unlikely that it could be caused entirely by crustal rocks, as the magnetization needed is too high. Likewise, it cannot be caused by a thin serpentinized layer at the base of the crust, because the combination of thickness and seismic velocity of this layer do not permit it to have a large enough magnetization or magnetic susceptibility. The intermediate wavelength signal should be capable of being measured by MAGSAT, which will then give a picture of the spatial arrangement of the intermediate wavelength anomalies, and hopefully a clue as to their origin.

Acknowledgements

We have benefitted from discussions with R.L. Parker. We thank Peter Rona, Bosco Loncarevic and the NGSTDC for providing the data used in this paper. Research supported by the National Science Foundation, Oceanography section. Contribution from the Rosenstiel School of Marine and Atmospheric Science, University of Miami.

Figure Captions

1. Locations of magnetic profiles. The EW Pacific profile is approximately 11,000 km long. The NS Pacific profile is approximately 13,000 km long. The Atlantic (TAG) profile is approximately 6,000 km long.
2. Total magnetic field recorded along the three profiles. In this and in other diagrams of magnetic field, the TAG profile is plotted from NW to SE (left to right), the EW Pacific is plotted with west on the left and the NS Pacific is plotted with south to the left.
3. Power spectrum of total magnetic field for the three profiles. The power is in $(nT)^2$.
4. Power spectrum of total magnetic field for the three profiles after application of a 4π prolate spheroidal filter.
5. First few power estimates from Figure 4 plotted on an expanded abscissa scale.
6. Position of the maximum value of the Earth filter as a function of depth to top, and thickness of the magnetized layer.
7. Power spectra for magnetizations generated by reversals of the field following a Poisson distribution. Examples for different combinations of spreading rate and reversal rate are shown. The parameter s is the average number of km/reversal, obtained by dividing the spreading rate (km/my) by the reversal rate (per my). The spectra are normalized to unity at zero wavenumber.
8. Power spectrum for Poisson (K = 1) and renewal (K = 2) processes.
9. Contribution to RMS field intensity for each degree of spherical harmonic. Two representations are shown (Barraclough et al., 1975; Peddie and Fabiano, 1976). They both give the same value to within the size of the symbols for degrees of harmonic less than 9.

10. Theoretical power spectrum for a combination of core field and a crustal field caused by reversals of magnetization. Two crustal field models are shown, for different reversal rates (μ), spreading rates (s) and thicknesses of magnetized material (d). The depth to the top of the magnetized layer is h.

11. Comparison between theoretical power spectra for crustal sources and the observed spectrum from the EW Pacific profile. The full smooth curve is for a reversal rate of 3.my^{-1}, a spreading rate of 30 km.my^{-1}, a top depth of 5 km and a bottom depth of 11 km. The dashed line is for a reversal rate of 4.my^{-1}, a spreading rate of 25 km.my^{-1}, a top depth of 5 km and a bottom depth of 5.5 km. All three spectra were made to agree at a wavenumber of 0.15 radians.km^{-1}.

12. Anomalous fields along each profile.

13. Power spectra for the three profiles after removing a regional field, which is supposed to represent the core field.

14. Magnetization for each profile.

15. Total magnetic field recorded at Toolangi and its power spectrum.

16. Magnetic anomalies continued upward to 350 km. Topographic profiles are also shown.

17. Average power per radian.km^{-1} for each of the profiles. Power has been calculated at intervals of 0.05 radian.km^{-1} (or 0.02 radian.km^{-1} at the low wavenumber end of the spectrum). Note that there are offsets of the power in each of the three figures, to separate the three spectra. (a) Power spectrum from total field multiplied by 4π spheroidal data window. (b) Power spectrum from anomalous field multiplied by 4π spheroidal data window. (c) Power spectrum from anomalous field.

References

Bott, M.H.P. and M.A. Hutton, A matrix method for interpreting oceanic magnetic anomalies, Geophys. J. Roy. astr. Soc. 20, 149-157, 1970.

Bott, M.H.P., Solution of the linear inverse problem in magnetic interpretation with application to oceanic magnetic anomalies, Geophys. J. Roy. astr. Soc. 13, 313-323, 1967.

Alldredge, L.R., G.D. van Voorhis and T.M. Davis, A magnetic profile around the world, J. Geophys. Res. 68, 3679-3692, 1963.

Barraclough, D.R., J.M. Harwood, B.R. Leaton and S.R.C. Malin, A model of the geomagnetic field at epoch 1975, Geophys. J. Roy. astr. Soc. 43, 645-659, 1975.

Bullard, E.C., Removal of trend from magnetic surveys, Earth Planet. Sci. Letts. 2, 293-300, 1967.

Cain, J.C., Structure and secular change of the geomagnetic field, in "Proceedings of the Takesi Nagata Conference", ed R.M. Fisher, M. Fuller, V.A. Schmidt and P.J. Wasilewski, Univ. Pittsburgh Press, 113-129, 1975.

Christensen, N.I., The abundance of serpentinites in the oceanic crust, J. Geol. 80, 709-719, 1972.

Coles, R.L. and G.V. Haines, Long-wavelength magnetic anomalies over Canada, using polynomial and upward continuation techniques, J. Geoelect. Geomagnet., in press.

Cox, A., Lengths of geomagnetic polarity intervals, J. Geophys. Res., 73, 101-112, 1968.

Cox, A., Symmetric and asymmetric geomagnetic reversals as a renewal process, in "Proceedings of the Takesi Nagata Conference", ed R.M. Fisher, M. Fuller, V.A. Schmidt and P.J. Wasilewski, Univ. Pittsburgh Press, 172-186, 1975.

Fox, P.J. and N.D. Opdkye, Geology of the oceanic crust: magnetic properties of oceanic rocks, J. Geophys. Res. 78, 5139-5154, 1973.

Hatherton, T., A geophysical study of Nelson-Cook Strait region, New Zealand, J. Geol. Geophys. N.Z. 10, 1330-1347, 1967.

Harrison, C.G.A., What is the true rate of reversals of the Earth's magnetic field? Earth Planet. Sci. Letts. 6, 186-188, 1969.

Harrison, C.G.A., Magnetization of the oceanic crust, Geophys. J. Roy. astr. Soc. 47, 257-284, 1976.

Irving, E., W.A. Robertson and F. Aumento, The mid-Atlantic ridge near 45°N. VI. Remanent intensity, susceptibility and iron content of dredged samples, Can. J. Earth Sci. 7, 226-238, 1970.

Keller, G.H. and G. Peter, East-west profile from Kermadec trench to Valparaiso, Chile, J. Geophys. Res. 73, 7154-7157, 1968.

Lattimore, R.K., P.A. Rona and O.E. DeWald, Magnetic anomaly sequence in the Central North Atlantic, J. Geophys. Res. 79, 1207-1209, 1974.

Lewis, B.T.R. and W.E. Syndsman, Evidence for a low velocity layer at the base of the oceanic crust, Nature 266, 340-344, 1977.

Lowes, F.J., Mean-square values on sphere of spherical harmonic vector fields, J. Geophys. Res. 71, 2179, 1966.

Lowes, F.J., Spatial power spectrum of the main geomagnetic field, and extrapolation to the core, Geophys. J. Roy. astr. Soc. 36, 717-730, 1974.

Naidu, P.S., Statistical structure of geomagnetic field reversals, J. Geophys. Res. 76, 2649-2662, 1971.

Nomura, M., Marine geomagnetic anomalies with intermediate wavelengths in the western Pacific region, Bull. Earthquake Res. Inst. 11, 1-42, 1979.

Peddie, N.W. and E.B. Fabiano, A model of the geomagnetic field for 1975, J. Geophys. Res. 81, 2539-2542, 1976.

Rice, S.O., Mathematical theory of random noise, selected papers on noise and stochastic processes, 133-294, ed Nelson Wax, Dover Publs., Inc., New York, 1954.

Saad, A.H., Magnetic properties of ultramafic rocks from Red Mountain, California, Geophys. 34, 974-987, 1969.

Schouten, H. and K. McCamy, Filtering marine magnetic anomalies, J. Geophys. Res. 77, 7089-7099, 1972.

Schouten, J.A., A fundamental analysis of magnetic anomalies over oceanic ridges, Mar. Geophys. Res. 1, 111-144, 1971.

Spector, A. and F.S. Grant, Statistical models for interpreting aeromagnetic data, Geophys. 35, 293-302, 1970.

Thomson, D.J., Spectrum estimation techniques for characterization of WT4 waveguide-I, Bell System Tech. J. 56, 1769-1815, 1977.

Table 1

Slopes of power spectra.

Profile	Wavenumber Range radians.km^{-1}			Slope, km	Standard Error, km
Atlantic, TAG	0.008	-	0.907	- 8.02	0.17
	0.008	-	1.006	- 8.21	0.15
	0.008	-	1.106	- 8.45	0.13
	0.008	-	1.206	- 8.59	0.12
Pacific, EW	0.0047	-	0.471	-10.25	0.48
	0.0047	-	0.558	-10.31	0.36
	0.0047	-	0.645	-10.00	0.29
	0.0047	-	0.732	- 9.68	0.24
	0.0047	-	0.820	- 9.74	0.20
Pacific, NS	0.0038	-	0.520	-10.31	0.33
	0.0038	-	0.614	- 9.72	0.24
	0.0038	-	0.708	- 9.78	0.19
	0.0038	-	0.801	- 9.93	0.16

Table 2

Average values of magnetization for each line.

Line	RMS magnetization, $A.m^{-1}$	Mean absolute magnetization, $A.m^{-1}$
Atlantic, TAG	0.81	0.60
Pacific, EW	1.73	1.32
Pacific, NS	1.78	1.35

Table 3

Power spectra.

	Total field (4π prolate spheroidal data window.)		Anomalous field (4π prolate spheroidal data window)		Anomalous field	
Profile	Intercept	Slope, km	Intercept	Slope, km	Intercept	Slope, km
Pacific, EW	12.3	-9.75	12.1	-9.20	11.8	-8.75
Pacific, NS	11.1	-9.75	11.1	-9.73	11.6	-8.40
Atlantic	10.8	-8.80	10.9	-9.11	10.7	-8.74

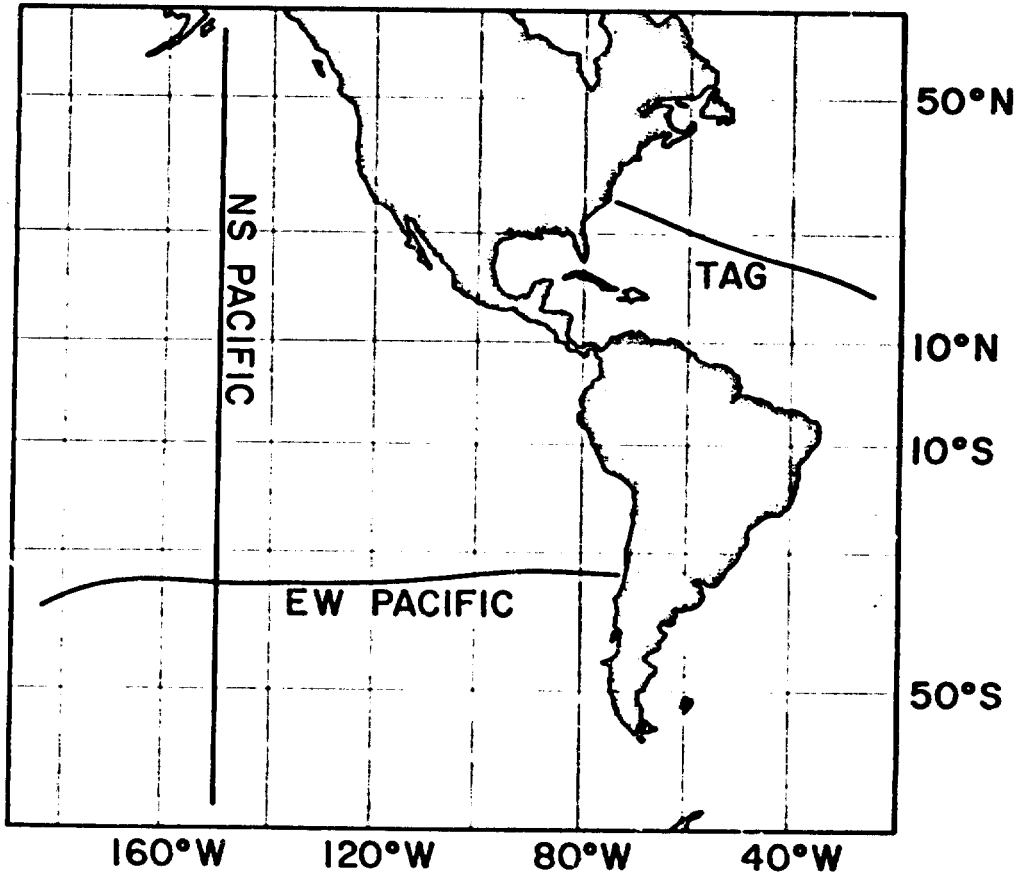

FIG 1

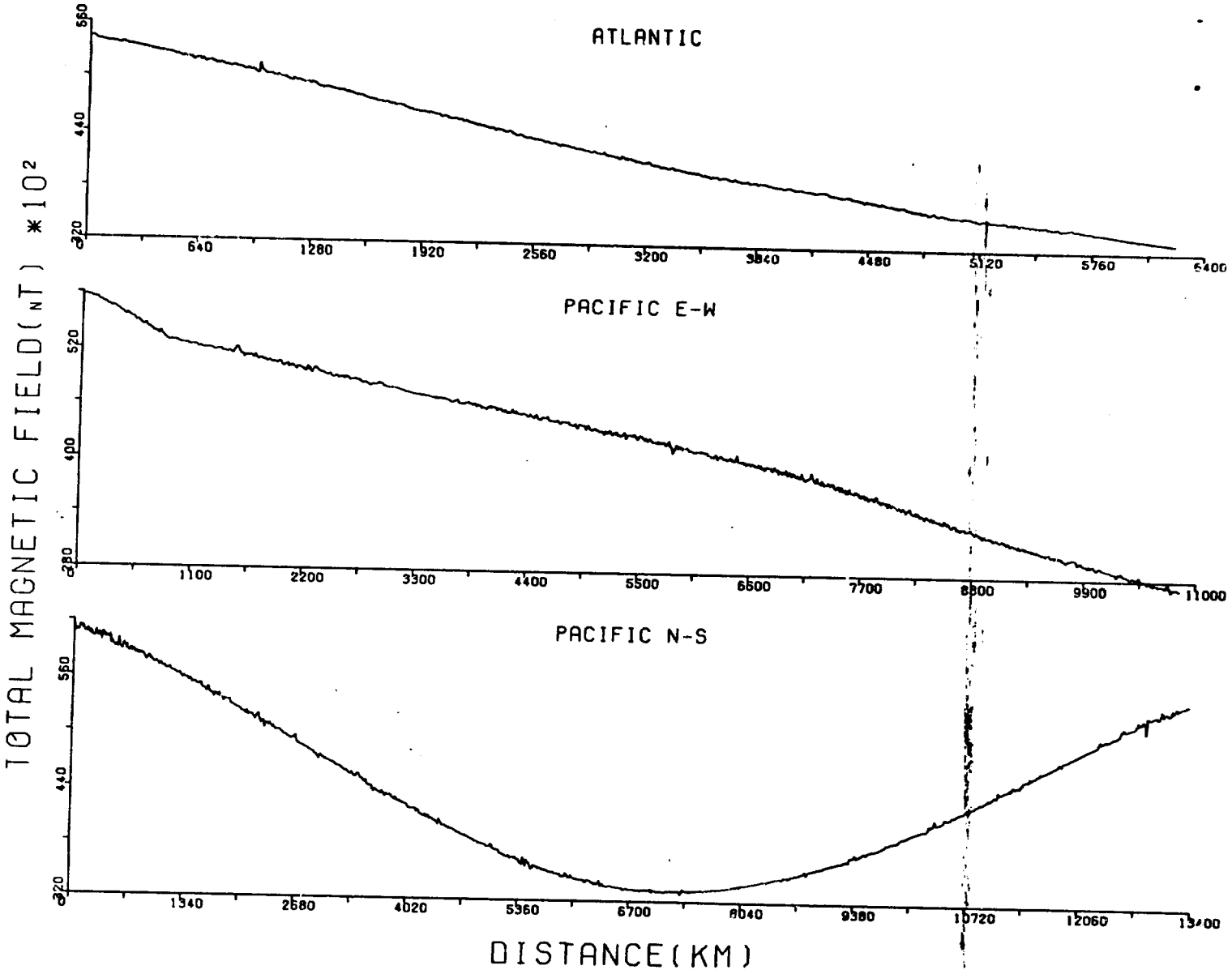
ATLANTIC
PACIFIC E-W
PACIFIC N-S
TOTAL MAGNETIC FIELD(nT) *10²
DISTANCE(KM)
560
440
320
640
1280
1920
2560
3200
3840
4480
5120
5760
6400
520
400
280
1100
2200
3300
4400
5500
6600
7700
8800
9900
11000
560
440
320
1340
2680
4020
5360
6700
8040
9380
10720
12060
13400

FIG 2

14

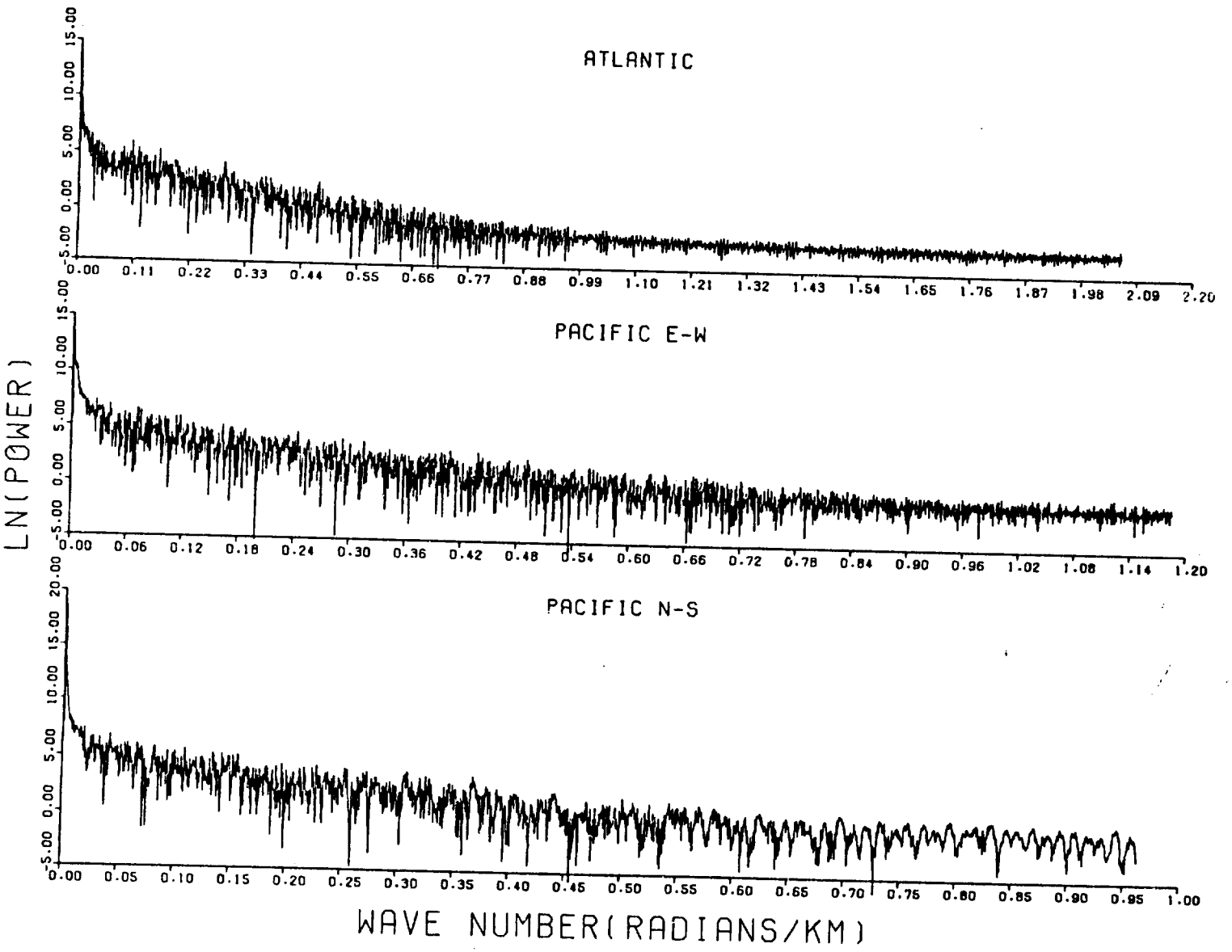
ATLANTIC
PACIFIC E-W
PACIFIC N-S
LN(POWER)
WAVE NUMBER(RADIANS/KM)

FIG 3

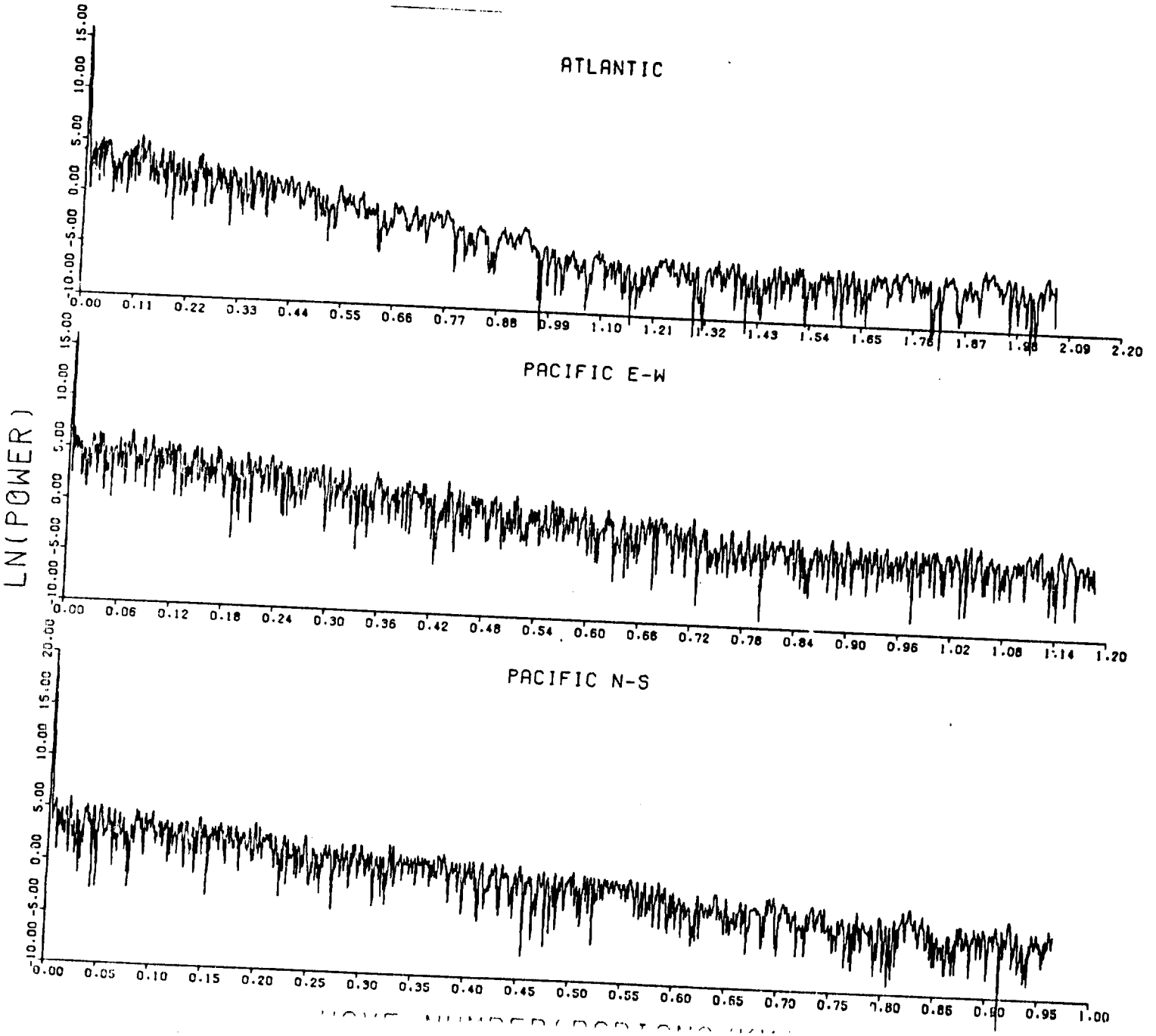
ATLANTIC
PACIFIC E-W
PACIFIC N-S
LN(POWER)
15.00
10.00
5.00
0.00
-5.00
-10.00
20.00
0.30
0.00 0.11 0.22 0.33 0.44 0.55 0.66 0.77 0.88 0.99 1.10 1.21 1.32 1.43 1.54 1.65 1.76 1.87 1.98 2.09 2.20
0.00 0.06 0.12 0.18 0.24 0.30 0.36 0.42 0.48 0.54 0.60 0.66 0.72 0.78 0.84 0.90 0.96 1.02 1.08 1.14 1.20
0.00 0.05 0.10 0.15 0.20 0.25 0.30 0.35 0.40 0.45 0.50 0.55 0.60 0.65 0.70 0.75 0.80 0.85 0.90 0.95 1.00

FIG 4

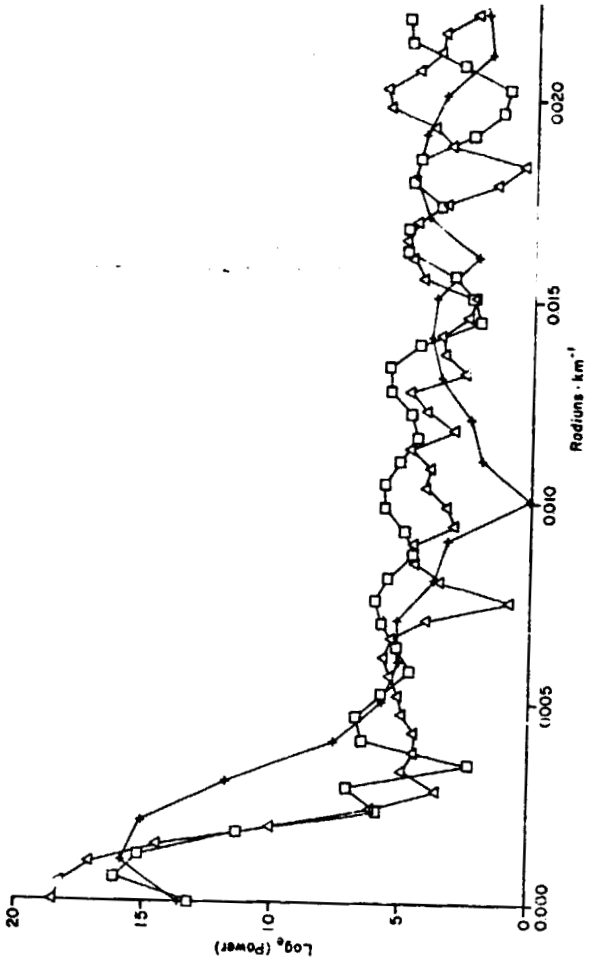

F16 5

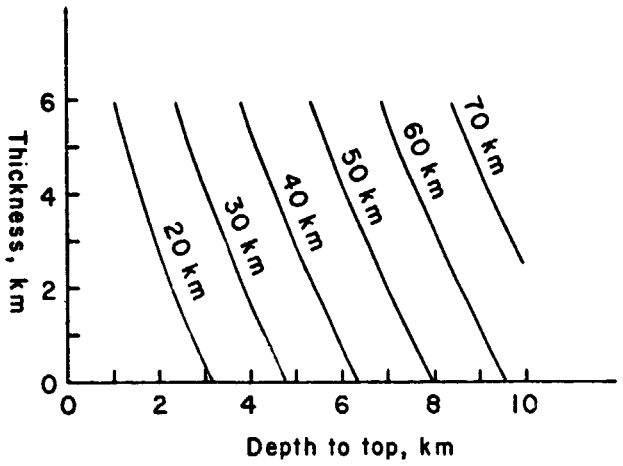
Thickness, km
0
2
4
6
0
2
4
6
8
10
Depth to top, km
20 km
30 km
40 km
50 km
60 km
70 km

FIG 6

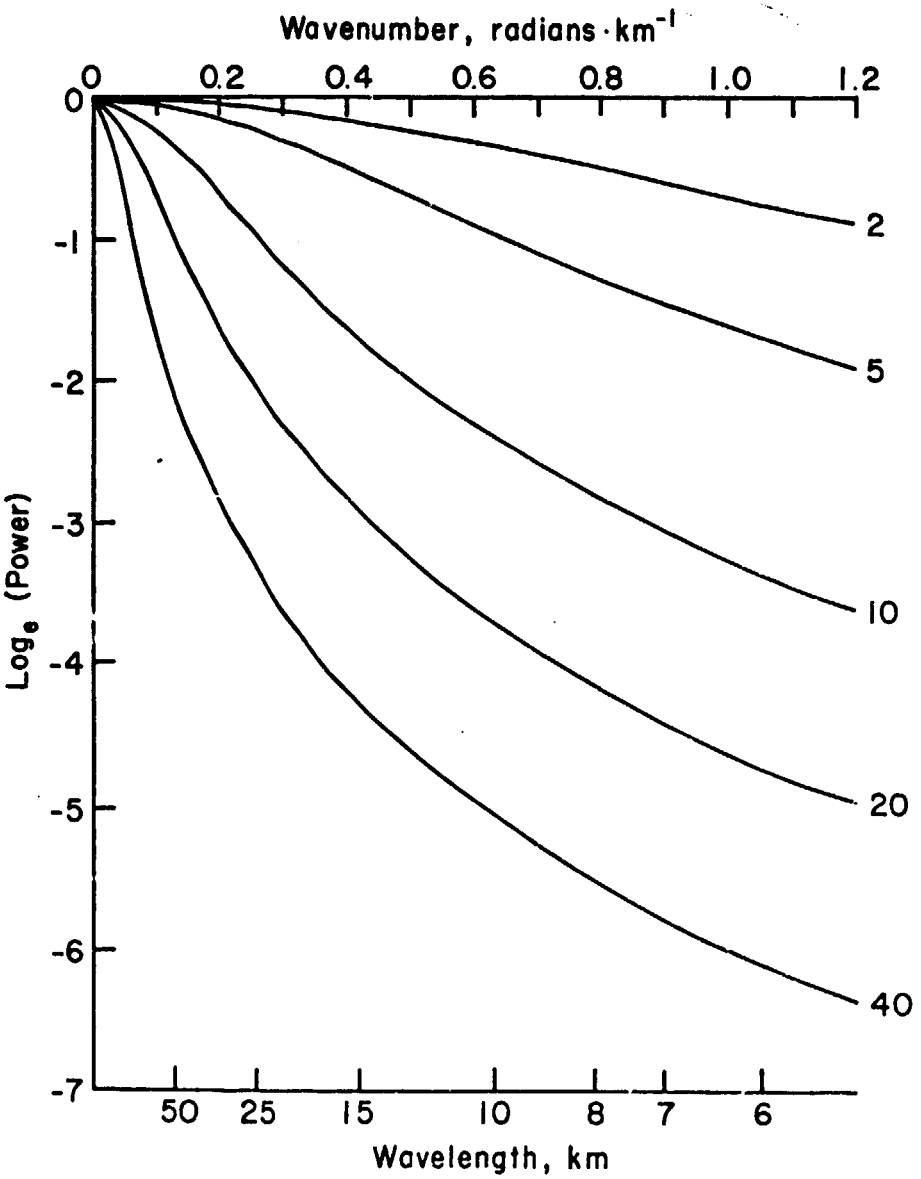
Wavenumber, radians · km⁻¹
0
0.2
0.4
0.6
0.8
1.0
1.2
0
-1
-2
-3
-4
-5
-6
-7
Log_e (Power)
2
5
10
20
40
50
25
15
10
8
7
6
Wavelength, km

FIG 7

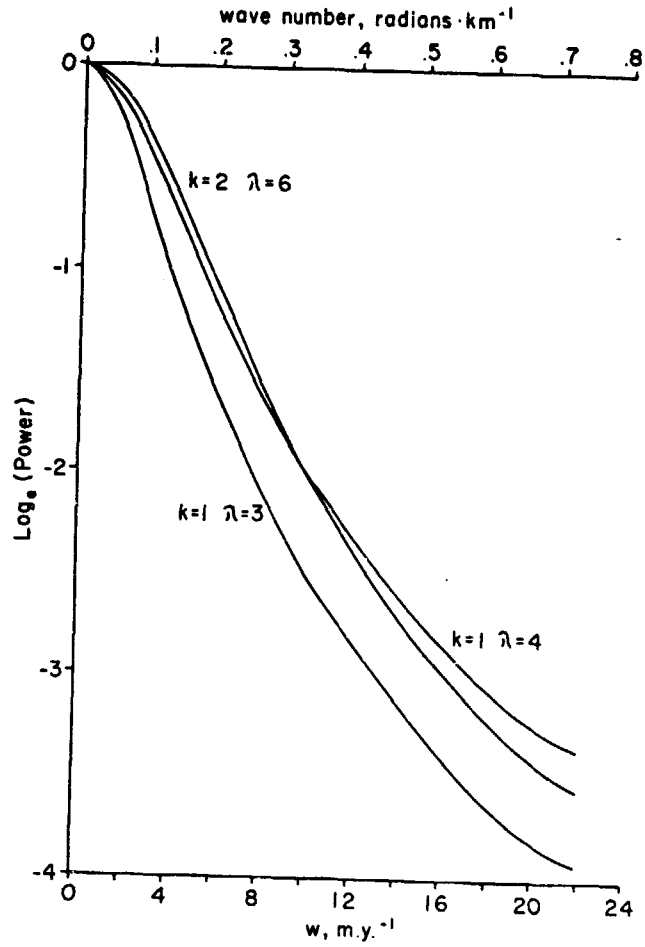
wave number, radians · km⁻¹
0
.1
.2
.3
.4
.5
.6
.7
.8
k=2 λ=6
k=1 λ=3
k=1 λ=4
Log$_e$ (Power)
-1
-2
-3
-4
0
4
8
12
16
20
24
w, m.y.⁻¹

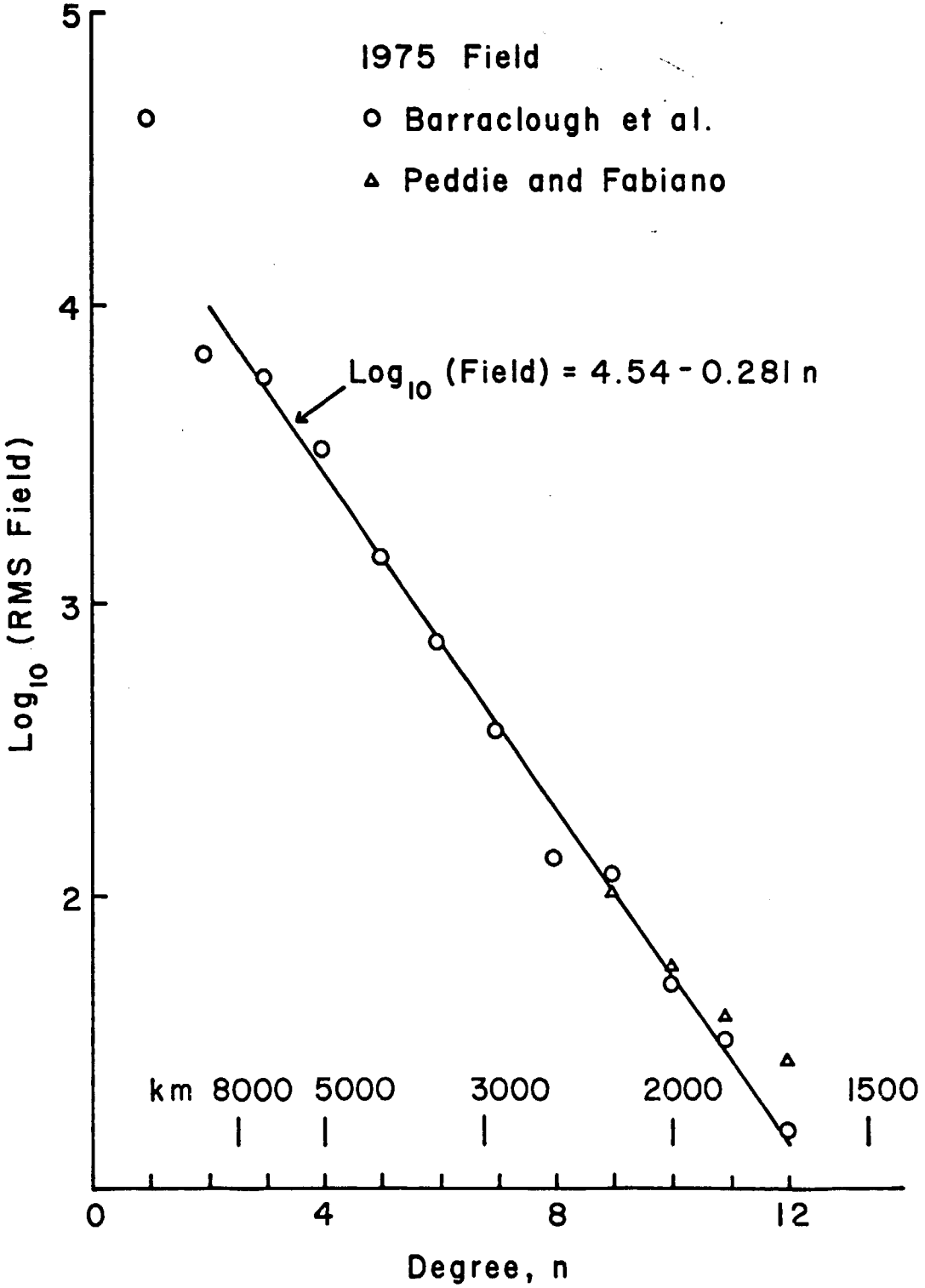
1975 Field
Barraclough et al.
Peddie and Fabiano
Log10 (Field) = 4.54 - 0.281 n
Log10 (RMS Field)
5
4
3
2
km 8000 5000 3000 2000 1500
0 4 8 12
Degree, n

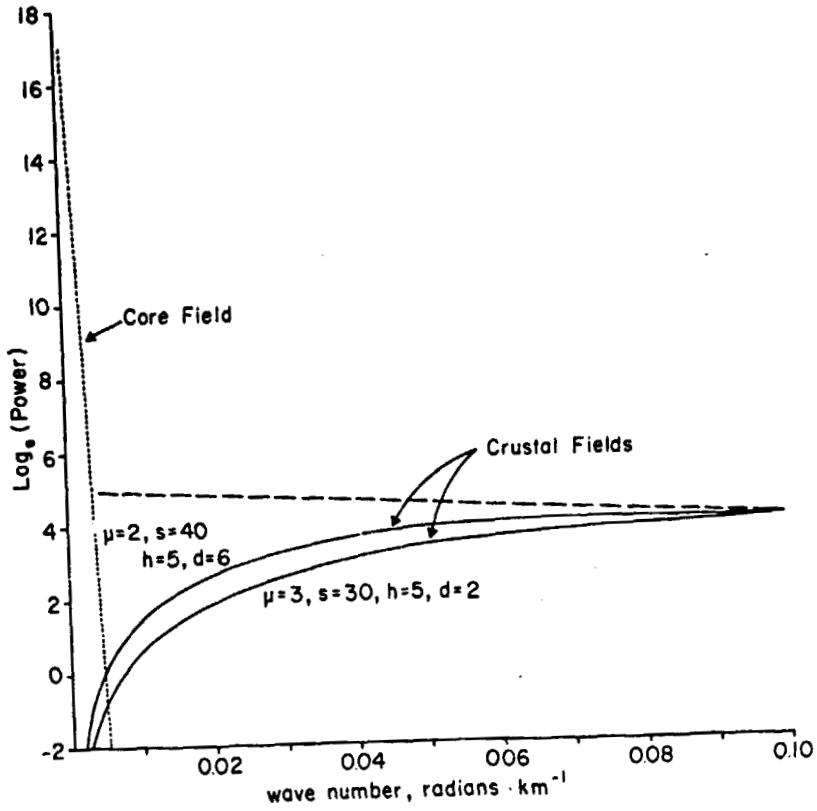

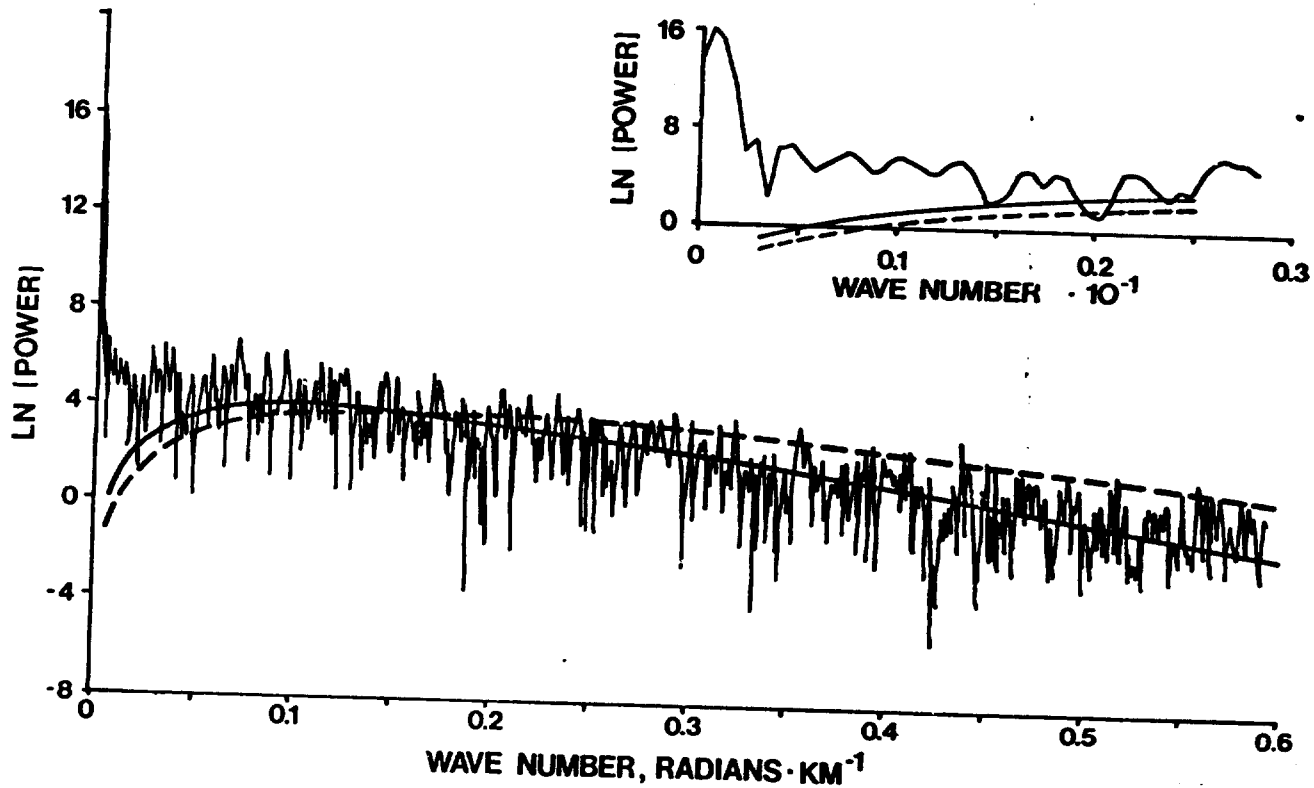
LN (POWER)
16
12
8
4
0
-4
-8
0
0.1
0.2
0.3
0.4
0.5
0.6
WAVE NUMBER, RADIANS · KM^{-1}
LN (POWER)
16
8
0
0
0.1
0.2
0.3
WAVE NUMBER · 10^{-1}

Fig 11

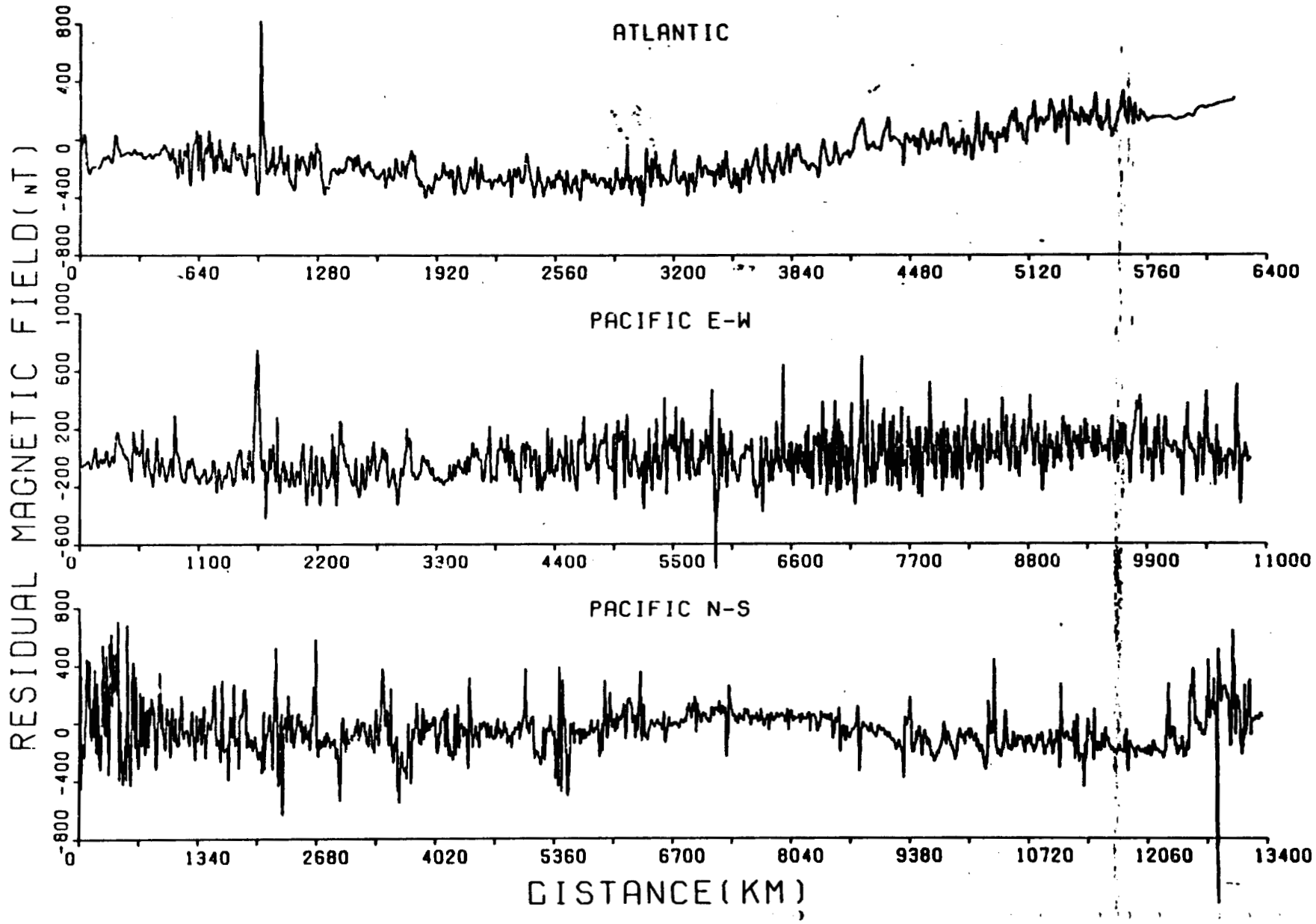
ATLANTIC
PACIFIC E-W
PACIFIC N-S
RESIDUAL MAGNETIC FIELD(nT)
DISTANCE(KM)
800
400
0
-400
-800
1000
600
200
-200
-600
0
640
1280
1920
2560
3200
3840
4480
5120
5760
6400
1100
2200
3300
4400
5500
6600
7700
8800
9900
11000
1340
2680
4020
5360
6700
8040
9380
10720
12060
13400

FIG-12

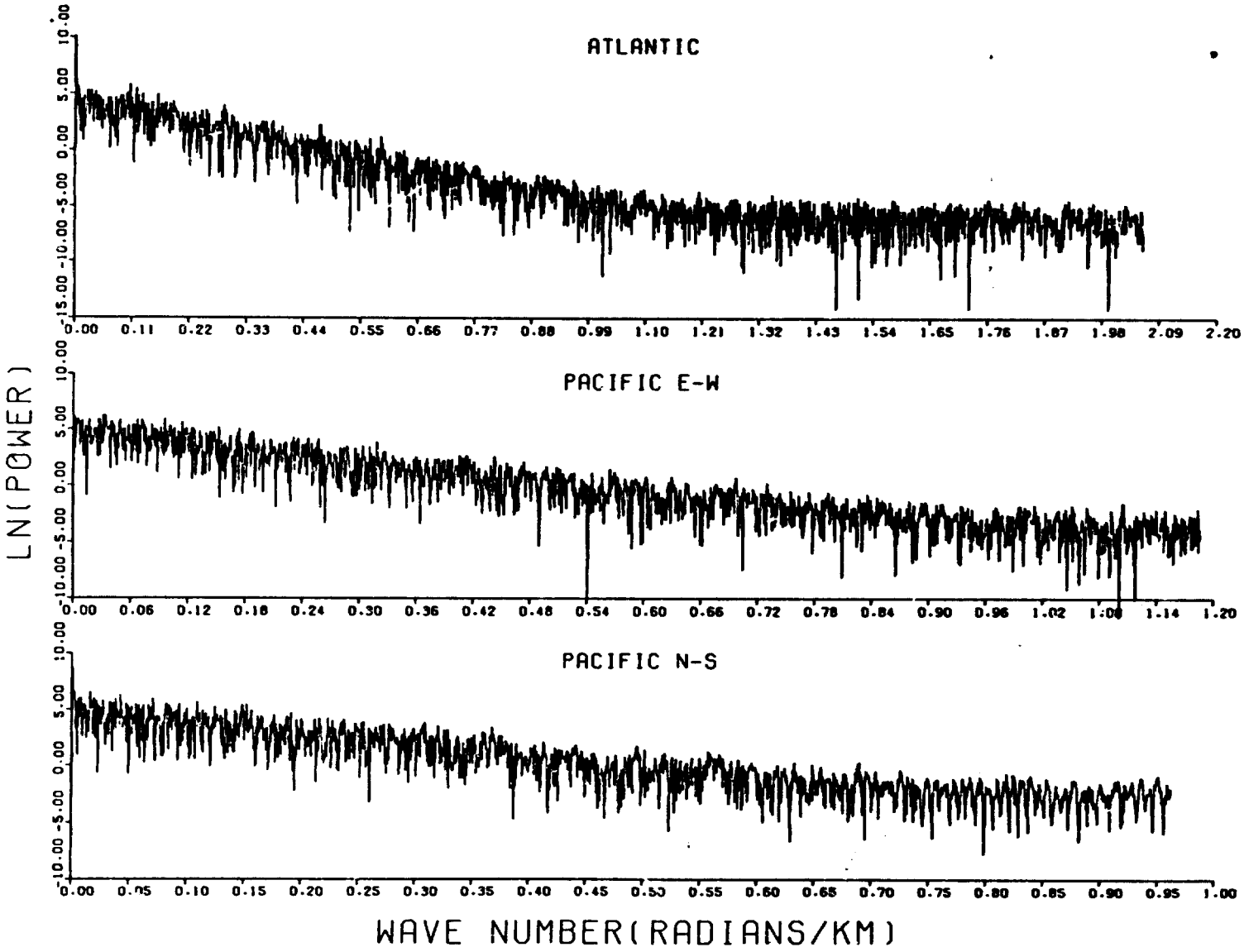
ATLANTIC
PACIFIC E-W
PACIFIC N-S
LN(POWER)
10.00
5.00
0.00
-5.00
-10.00
-15.00
0.00 0.11 0.22 0.33 0.44 0.55 0.66 0.77 0.88 0.99 1.10 1.21 1.32 1.43 1.54 1.65 1.76 1.87 1.98 2.09 2.20
0.00 0.06 0.12 0.18 0.24 0.30 0.36 0.42 0.48 0.54 0.60 0.66 0.72 0.78 0.84 0.90 0.96 1.02 1.08 1.14 1.20
0.00 0.05 0.10 0.15 0.20 0.25 0.30 0.35 0.40 0.45 0.50 0.55 0.60 0.65 0.70 0.75 0.80 0.85 0.90 0.95 1.00
WAVE NUMBER(RADIANS/KM)

Fig 13

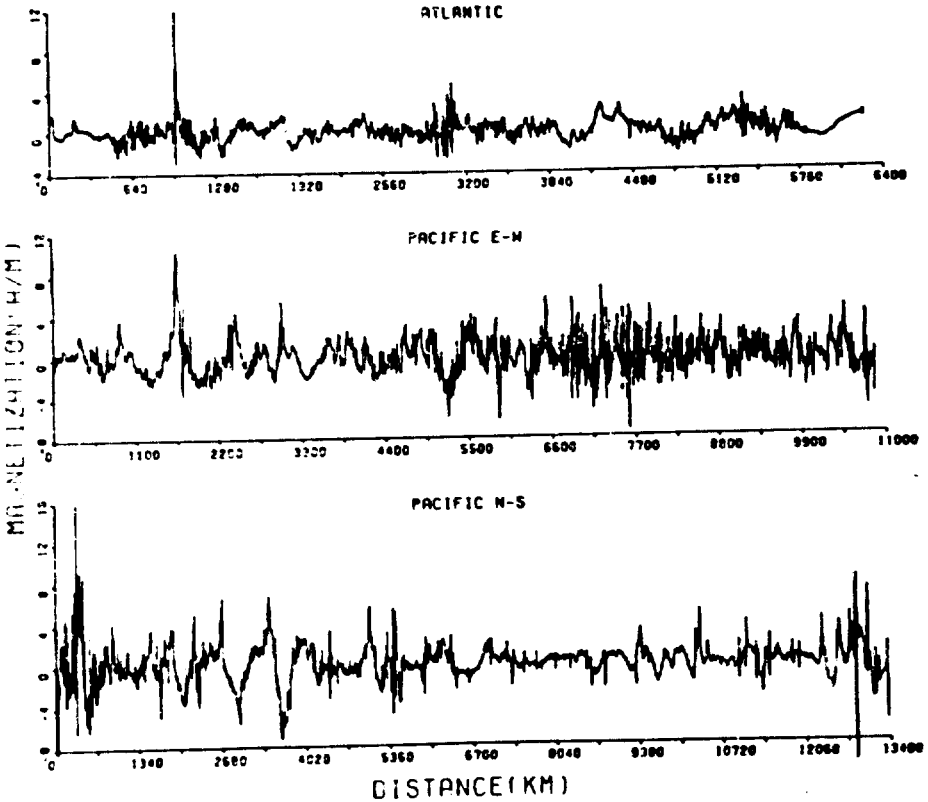

FIG 14

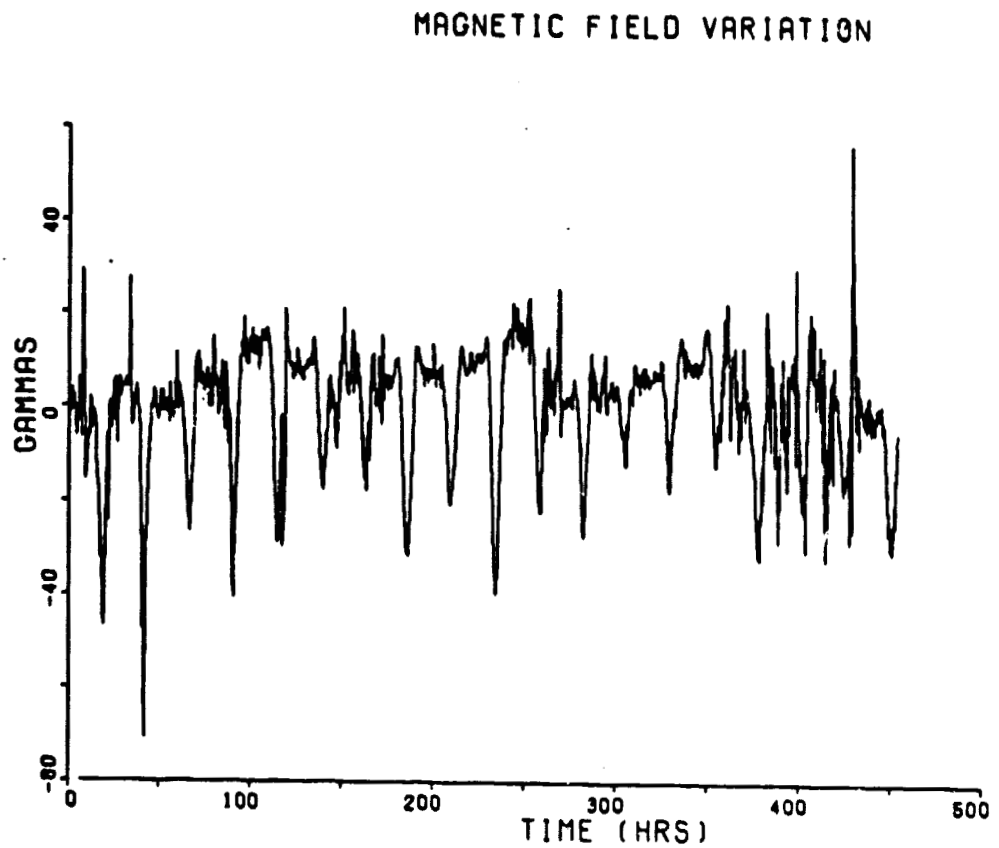

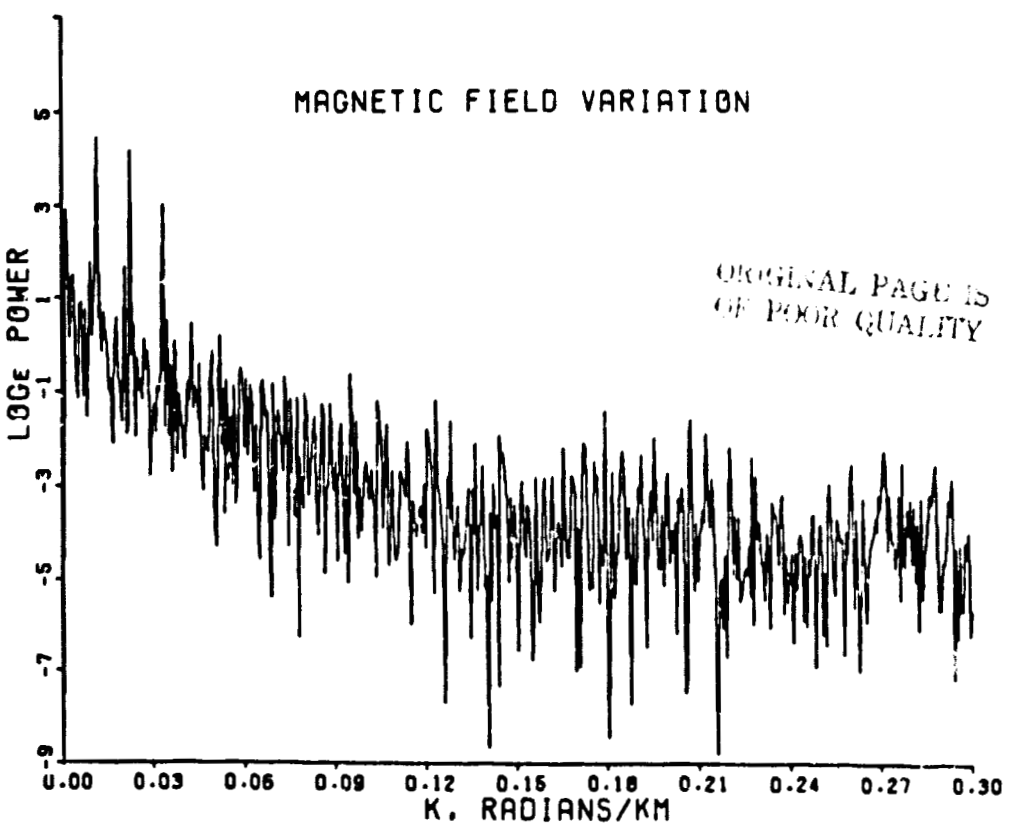

FIG 15

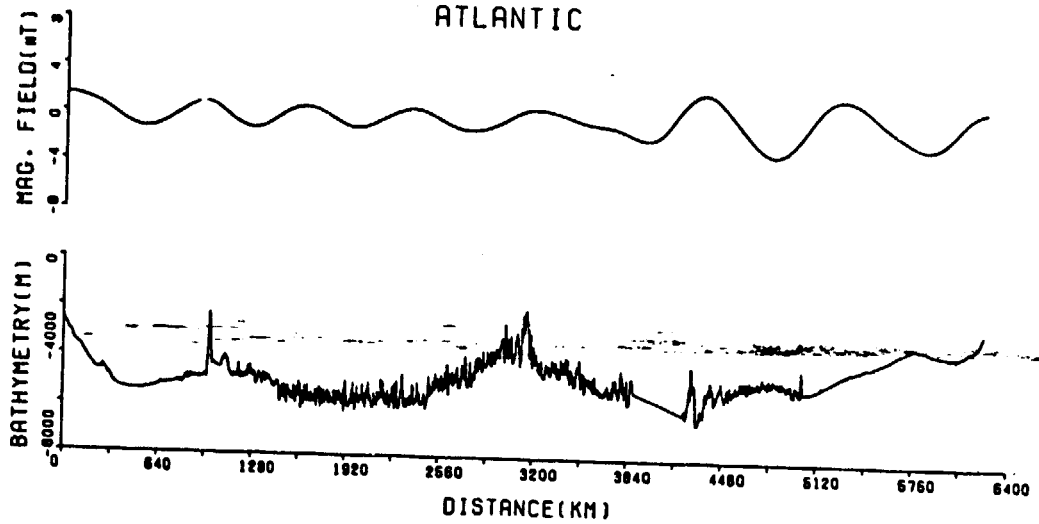
ATLANTIC
MAG. FIELD(nT)
8
4
0
-4
-8
BATHYMETRY(M)
0
-4000
-8000
0
640
1280
1920
2560
3200
3840
4480
5120
5760
6400
DISTANCE(KM)

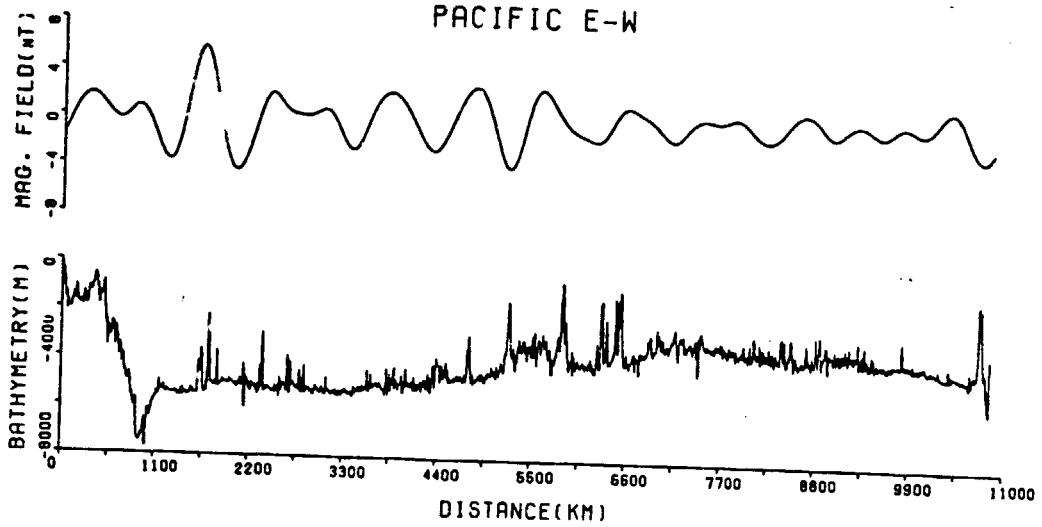
PACIFIC E-W
MAG. FIELD(nT)
8
4
0
-4
-8
BATHYMETRY(M)
0
-4000
-8000
0
1100
2200
3300
4400
5500
6600
7700
8800
9900
11000
DISTANCE(KM)

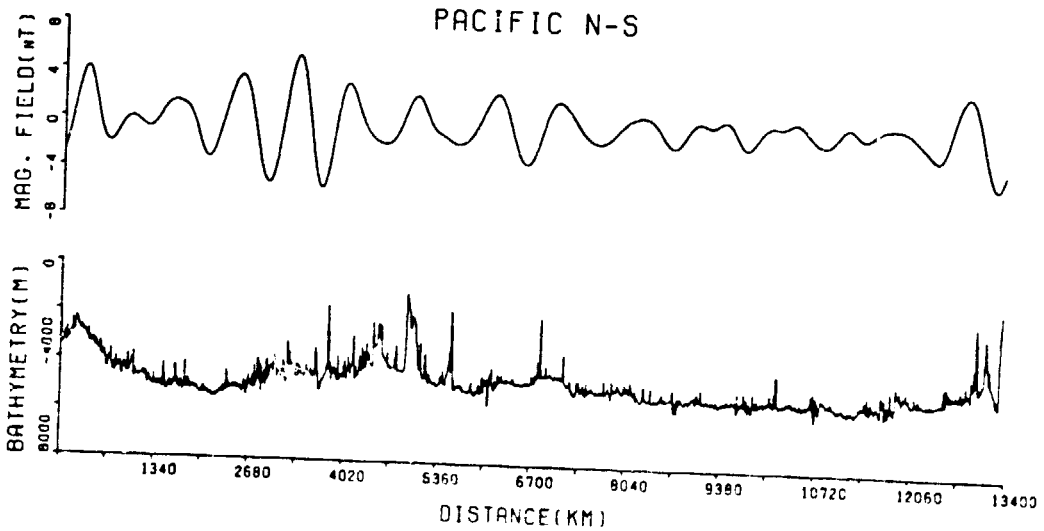
PACIFIC N-S
MAG. FIELD(nT)
8
4
0
-4
-8
BATHYMETRY(M)
0
-4000
-8000
1340
2680
4020
5360
6700
8040
9380
10720
12060
13400
DISTANCE(KM)

FIG 16

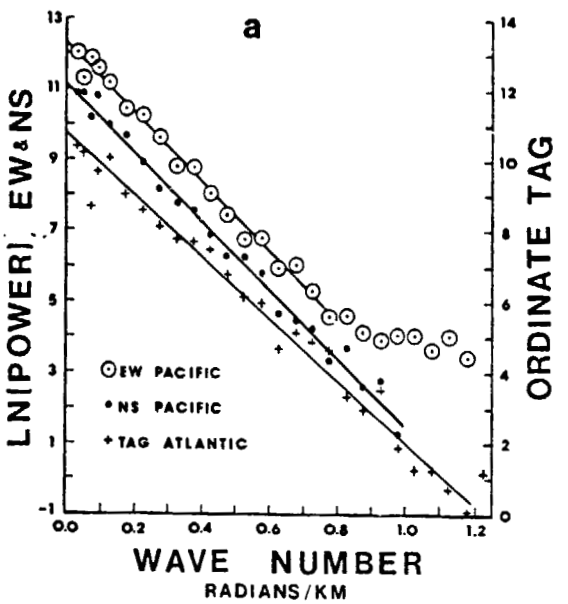

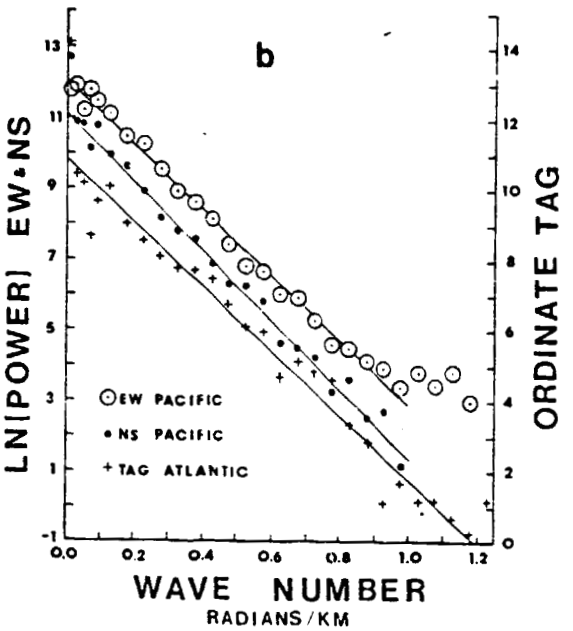

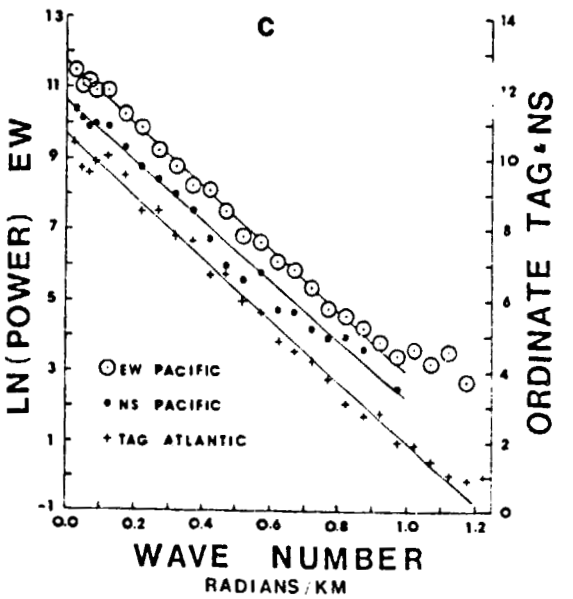

Fig 17